A NUMERICAL SIMULATION OF THERMAL AND ELECTRICAL PROPERTIES OF NANO-FIBER NETWORK POLYMER COMPOSITES USING PERCOLATION THEORY AND MONTE CARLO METHOD

A Thesis

by

HENG GU

Submitted to the Office of Graduate Studies of
Texas A&M University
in partial fulfillment of the requirements for the degree of

MASTER OF SCIENCE

December 2008

Major Subject: Mechanical Engineering

A NUMERICAL SIMULATION OF THERMAL AND ELECTRICAL PROPERTIES OF NANO-FIBER NETWORK POLYMER COMPOSITES USING PERCOLATION THEORY AND MONTE CARLO METHOD

A Thesis

by

HENG GU

Submitted to the Office of Graduate Studies of
Texas A&M University
in partial fulfillment of the requirements for the degree of

MASTER OF SCIENCE

Approved by:

Chair of Committee,	Choongho Yu
Committee Members,	Raymundo Arroyave
	Hae-Kwon Jeong
Head of Department,	Dennis O'Neal

December 2008

Major Subject: Mechanical Engineering

ABSTRACT

A Numerical Simulation of Thermal and Electrical Properties of Nano-fiber Network Polymer Composites Using Percolation Theory and Monte Carlo Method.

(December 2008)

Heng Gu, B.A., Nanjing University of Science & Technology;

M.S., Ruhr University Bochum

Chair of Advisory Committee: Dr. Choongho Yu

Polymer matrix composites reinforced by metal fibers are observed to present an onset of the insulator-to-conductor transition through previous experimental studies. Analytical studies revealed that the percolation threshold occurs when fiber volume fraction reaches the critical value. The numerical study based on Monte Carlo simulations are performed to investigate such a relation. In this work, the conductive fillers are modeled as a three dimensional (3D) network of identical units randomly distributed in the polymer matrix. For the simplest case, straight fibers are used in the simulation. The effects of the aspect ratio and fiber length on the critical volume fraction are also studied. Linearization is made to the logarithm of simulation results. Next, in order to study the effects of emulsion particles and the emulsion particle sizes on the percolation behavior, cubic particles are aligned in the sample model. The gap width to particle size ratio is fixed at 1/10. The calculated critical volume fraction is used in the power-law function to predict the electrical conductivity of the polymer

composites. Due to the insensitivity of the thermal conductivity to the percolation threshold, a combination of two empirical equations is used to predict the range of overall thermal conductivity.

DEDICATION

To my parents who always supported and encouraged me when I experienced tension, doubt, and frustration. To all the others who are warm-hearted and helped me.

ACKNOWLEDGEMENTS

I would like to express my sincere gratitude to my advisor, Dr. Choongho Yu, assistant professor and director of the Nano Energy lab in the Department of Mechanical Engineering at Texas A&M University. His constructive suggestions and logical thinking were of great value to me. In addition, the thoughtful discussions with Dr. Raymundo Arroyave and Dr. Hae-Kwon Jeong were very helpful to this work. The support from the supercomputing center at Texas A&M University is also highly appreciated.

TABLE OF CONTENTS

Page

LIST OF FIGURES

FIGURE Page

LIST OF TABLES

CHAPTER I

INTRODUCTION

Composites are defined as structures made of materials which maintain their identities even after the component is fully formed. The ingredients of the composites are usually with significantly different physical or chemical properties and remain separate and distinct on a macroscopic level within the finished structure. There are two categories of constituent materials: matrix and reinforcement. At least one portion of each type is required. The matrix material surrounds and supports the reinforcement materials by maintaining their relative positions. The reinforcements impart their special mechanical and physical properties to enhance the matrix properties. Composites can be categorized by their matrix phase: metal matrix composites, ceramic matrix composites and polymer matrix composites; or by their reinforcement phase: particle reinforced composites and fiber reinforced composites.

1.1 Polymer matrix composites

Polymer matrix composites (PMCs) are of two broad types, thermosets and thermoplastics. Thermosets are solidified by irreversible chemical reactions, in which the molecules in the polymer “cross-link,” or form connected chains. The most common thermosetting matrix materials for high-performance composites used in the aerospace

---

This thesis follows the style of Composites Science and Technology.

industry are the epoxies. Thermoplastics, on the other hand, are melted and then solidified, a process that can be repeated numerous times for reprocessing. Although the manufacturing technologies for thermoplastics are generally not as well developed as those for thermosets, thermoplastics offer several advantages. First, they do not have the shelf-life problem associated with thermosets, which require freezer storage to halt the irreversible curing process that begins at room temperature. Second, they are more desirable from an environmental point of view, as they can be recycled. They also exhibit higher fracture toughness and better resistance to solvent attack. Unfortunately, thermoplastics are more expensive, and they generally do not resist heat as well as thermosets; however, strides are being made in developing thermoplastics with higher melting temperatures. Overall, thermoplastics offer a greater choice of processing approaches, so that the process can be determined by the scale and rate of production required and by the size of the component.

A variety of reinforcements can be used with both thermoset and thermoplastic PMCs, including particles, whiskers (very fine single crystals), discontinuous (short) fibers, continuous fibers, and textile preforms (made by braiding, weaving, or knitting fibers together in specified designs). Continuous fibers are more efficient at resisting loads than are short ones, but it is more difficult to fabricate complex shapes from materials containing continuous fibers than from short-fiber or particle-reinforced materials. To aid in processing, most high-performance composites are strengthened with filaments that are bundled into yarns. Each yarn, or tow, contains thousands of filaments, each of which has a diameter of approximately 10 micrometers (0.01 millimeter, or 0.0004 inch).

Depending on the application and on the type of load to be applied to the composite part, the reinforcement can be random, unidirectional (aligned in a single direction), or multidirectional (oriented in two or three dimensions). If the load is uniaxial, the fibers are all aligned in the load direction to gain maximum benefit of their stiffness and strength. However, for multidirectional loading (for example, in aircraft skins), the fibers must be oriented in a variety of directions. This is often accomplished by stacking layers (or lamina) of continuous-fiber systems.

Carbon nanotubes are graphitic sheets rolled into seamless tubes (i.e., arrangements of carbon hexagons into tube-like fullerenes) and have diameters ranging from about a nanometer to tens of nanometers with lengths up to centimeters. Nanotubes have received much attention due to their interesting properties (high modulus and electrical/thermal conductivity) since their discovery by Iijima in 1991 [1, 2]. Since then, significant effort has been made to incorporate nanotubes into conventional materials (such as polymers) for improved strength and conductivity [3~12]. Moreover, many potential applications have been proposed for carbon nanotubes, including conductive and high-strength composites; energy storage and energy conversion devices; sensors; field emission displays and radiation sources; hydrogen storage media and nanometer-sized semiconductor devices; probes and interconnects [13].

Nanotubes can be synthesized in two structural forms, single-wall and multiwall (as shown in Fig. 1). The first tubules Iijima discovered exhibited the multiwall structure of concentric nanotubes forming one tube defining a multiwall nanotube (MWNT) (with a constant interlayer separation of 0.34A) [1].

1.2 Manufacturing process

Fiber-reinforced nanocomposites are manufactured through affordable RTM, and VARTM processes described in different literatures [14-17]. Hussain et al. [15] achieved an almost (by dispersing only 1% by weight nanosilicates) 18 and 24% improvement in flexural strength and fracture toughness respectively in S2 glass/ vinylester−clay nanocomposites compared to conventional composites [15]. Roy and Hussain [18,19] manufactured E-glass/PP clay nanocomposites using prepreg tapes with extruder and pultrusion machine. They achieved improvements in compressive strength and modulus using this technique. Fielding et al. [14] achieved uniform dispersion of the nanoclay of carbon fiber reinforced epoxy nanocomposites using RFI in the autoclave.

The most common form of material used for the fabrication of composite structures is the preimpregnated tape, or “prepreg.” There are two categories of prepreg: tapes, generally 75 millimeters (3 inches) or less in width, intended for fabrication in automated, computer-controlled tape-laying machines; and “broad goods,” usually several meters in dimension, intended for hand lay-up and large sheet applications. To make prepregs, fibers are subjected to a surface treatment so that the resin will adhere to them. They are then placed in a resin bath and rolled into tapes or sheets.

To fabricate the composite, the manufacturer “lays up” the prepreg according to the reinforcement needs of the application. This has traditionally been done by hand, with successive layers of a broad-goods laminate stacked over a tool in the shape of the desired part in such a way as to accommodate the anticipated loads. However, efforts are now being directed toward automated fiber-placement methods in order to reduce

costs and ensure quality and repeatability. Automated fiber-placement processes fall into two categories, tape laying and filament winding. The tape-laying process involves the use of devices that control the placement of narrow prepreg tapes over tooling with the contours of the desired part and along paths prescribed by the design requirements of the structure. The width of the tape determines the “sharpness” of the turns required to place the fibres in the prescribed direction—i.e., wide tapes are used for gradual turns, while narrow tapes are required for the sharp turns associated with more complex shapes.

Filament winding uses the narrowest prepreg unit available—the yarn, or tow, of impregnated filaments. In this process, the tows are wound in prescribed directions over a rotating mandrel in the shape of the part. Successive layers are added until the required thickness is reached. Although filament winding was initially limited to geodesic paths (i.e., winding the fibers along the most direct route between two points), the process is now capable of fabricating complex shapes through the use of robots.

For thermosetting polymers, the structure generated by either tape laying or filament winding must undergo a second manipulation in order to solidify the polymer through a curing reaction. This is usually accomplished by heating the completed structure in an autoclave, or oven. Thermoplastic systems offer the advantage of on-line consolidation, so that the high energy and capital costs associated with the curing step can be eliminated. For these systems, prepreg can be locally melted, consolidated, and cooled at the point of contact so that a finished structure is produced. A variety of energy sources are used to concentrate heat at the point of contact, including hot-gas torches, infrared light, and laser beams.

Pultrusion, the only truly continuous process for manufacturing parts from PMCs, is economical but limited to the production of beamlike shapes. On a pultrusion line, fibers and the resin are pushed through a heated die, or shaping tool, at one end, then cooled and pulled out at the other end. This process can be applied to both thermoplastic and thermoset polymers.

Resin transfer molding, or RTM, is a composites processing method that offers a high potential for tailorability but is currently limited to low-viscosity (easily flowing) thermosetting polymers. In RTM, a textile preform—made by braiding, weaving, or knitting fibers together in a specified design—is placed into a mold, which is then closed and injected with a resin. After consolidation, the mold is opened and the part removed. Preforms can be made in a wide variety of architectures, and several can be joined together during the RTM process to form a multi-element preform offering reinforcement in specific areas and load directions.

The similarity of meltable thermoplastic polymers to metals has prompted the extension of techniques used in metalworking. Sheet forming, used since the 19th century by metallurgists, is now applied to the processing of thermoplastic composites. In a typical thermoforming process, the sheet stock, or preform, is heated in an oven. At the forming temperature, the sheet is transferred into a forming system, where it is forced to conform to a tool, with a shape that matches the finished part. After forming, the sheet is cooled under pressure and then removed. Stretch forming, a variation on thermoplastic sheet forming, is specifically designed to take advantage of the extensibility, or ability to be stretched, of thermoplastics reinforced with long, discontinuous fibers. In this process, a straight preconsolidated beam is heated and then

stretched over a shaped tool to introduce curvature. The specific advantage of stretch forming is that it provides an automated way to achieve a very high degree of fibre-orientation control in a wide range of part sizes.

1.3 Applications

PMCs are valued in the aerospace industry for their stiffness, lightness, and heat resistance (see materials science: Polymer-matrix composites). They are fabricated materials in which carbon or hydrocarbon fibers (and sometimes metallic strands, filaments, or particles) are bonded together by polymer resins in either sheet or fiber-wound form. In the former, individual sheet elements are layered in metal, wood, or plastic molds and joined with adhesives. Applications for sheet composites include wing skins and fuselage bulkheads in aircraft and the underlying support for solar arrays in satellites. In fiber-wound forms, tubular or spherical shapes are fabricated by winding continuous fiber on a spinning mold (mandrel) with high-speed, computer-programmed precision, injecting liquid resin as the part is formed, and then curing the resin. This process is used for forming rocket motor casings; spherical containers for fuels, lubricants, and gases; and ducts for aircraft environmental systems.

Military aircraft demand lightweight structures to achieve high performance. Moreover, the materials used must be able to withstand the temperatures created by air friction when the vehicle is flying at high speeds. These requirements have fostered the use of new metals such as aluminum-magnesium alloys and titanium, as well as composites and polymers for many surfaces—as much as 35 percent of the structure (see materials science: Materials for aerospace). The manufacture of these materials and

their products has created new challenges. Titanium, although a relatively brittle material, has high strength-to-weight properties at operating temperatures as high as 480 °C (900 °F). Forming it into sheets generally requires heated dies and specialized machining and grinding. Titanium is therefore usually limited to applications, such as leading edges for wings and tails and related fittings, where its characteristics excel. Composites, on the other hand, are increasingly becoming staples of aircraft outer surfaces; thus, most structure manufacturers incorporate the necessary fabrication technology in their factories. To achieve required strengths, composite materials must be bonded in either hot- or cold-cure processes. Bonding is achieved within a vacuum, supplied either within evacuated rubberized bags or in autoclaves (temperature- and pressure-controlled chambers). Complementing the fabrication of composite sheets and fiber-wound forms is a comparatively recent method called pultrusion, which extrudes composite shapes in much the same fashion as molten metals are forced through a die. Other composite-making techniques incorporate the kind of ultra-light structural practices used with metals and fiberglass, such as sandwich construction.

In semiconductor industry, Electronic components such as integrated circuit chips can generate sufficient heat so that a heat dissipation arrangement must be provided. A common expedient for this purpose is to transfer heat from the component using a thermally conductive member, for example an integrated heat spreader and/or a heat sink, thermally connected to the circuit board or component. A thermal interface material (TIM) is used between the component or circuit board and the thermally conductive member to establish thermal contact and lower the thermal resistance. The

TIM technologies used for electronic packages also encompass several classes of materials such as phase change materials, epoxies, greases, and gels.

Due to the increasing performance demands for electronic components such as microprocessors, improving heat dissipation is one of the central issues. The recent trend in microprocessor architecture has been to increase the number of transistors (higher power), shrink processor size (smaller die), and increase clock speeds (high frequency) in order to meet the market demand for high performance microprocessors. These have resulted in the escalation of both the raw power as well as the power density (hot spots) at the silicon die level, which increase the demand for effective means of heat dissipation.

High performance, high power processors require the use of integrated heat spreaders. The well-known thermal greases, epoxies and phase change TIM materials that are currently available in the market do not meet the performance requirement for packages comprising an integrated heat spreader. In response, highly conductive, low modulus, cross-linked gel TIMs were developed.

In recent years, a new method was developed to improve the thermal conductivity of gel TIM polymer systems by incorporating carbon micro-fibers, with other fillers, in the thermal interface material. Other solutions to the demand for increasingly effective heat dissipation have also been proposed. By means of mechanical standoffs, the TIM gap is reduced to provide a shorter heat transfer path and thereby a reduction in the thermal resistance of the TIM. Improvements in packaging design include those approaches, which is newly developed and account for varying amounts of heat generated by separate chips within a package. Imparting a consistent

TIM thickness and thereby allowing the uniform transfer of heat are named advantages of the techniques for the application of TIMs by screen printing the TIM composition upon a substrate to form a layer followed by curing the layer. Such methods are also presented in the past decade.

A method of making a heat dissipation arrangement involving the formation of a gel pad on the inner surface of a heat spreader to cover exposed faces of chips on a circuit board is described in many most recent publications. Properties of the gel pad are specified to dissipate heat while at the same time physically protecting the chip from mechanical stresses or avoiding the transmission of such stresses to the bare silicon chips. A cured gel TIM to form the pad is specified to have a cohesive strength greater than its adhesive strength, a compressive modulus of less than 1.38 MPa, and a thermal conductivity of greater than 1.0 W/m° C.

Gel TIMs typically comprise a crosslinkable silicone polymer, such as a vinyl-terminated silicone oil, a crosslinker, such as a silane hydride crosslinker, and a thermally conductive filler. Before cure, these materials have properties similar to greases. They have high bulk thermal conductivities and low surface energies, and they conform well to surface irregularities upon dispense and assembly, which contributes to thermal contact resistance minimization. After cure, gel TIMs are crosslinked, filled polymers, and the crosslinking reaction provides cohesive strength to circumvent the pump-out issues exhibited by greases during temperature cycling. Their modulus (E) is low enough (on the order of mega-pascal, MPa, range compared to giga-pascal, GPa, range observed for epoxies) that the material can still dissipate internal stresses and

prevent interfacial delamination. Thus, the low modulus properties of these filled gels are attractive from a material integration standpoint.

However, it is often found that maintaining low thermal interface resistance in electronic packages employing gel TIMs currently used in the industry, is difficult. This is especially true for organic flip-chip packages, which introduce significant thermal-mechanical stress on the thermal interface material during reliability stress testing from the relative flexing of the die and the heat spreader with changes in temperature due to the differences in their coefficients of thermal expansion. One of the main technical challenges for gel TIM formulation is optimizing the mechanical properties such that the cured gel dissipates the thermal-mechanical stresses that arise due to the mismatch of thermal expansion coefficients of the chip and heat spreader, to thereby avoid delamination of the gel TIM. There is in need for improved electronic packages comprising a gel TIM, whose reliability meets not only the end of line package performance requirements but also the end of life performance requirements.

1.4 Prospects

In future, more attention will be paid to polymer matrix composites reinforced by nano-sized fillers. The potential of such nanocomposites in various sectors of research and application is promising and attracting increasing investment from Governments and business in many parts of the world. While there are some niche applications where nanotechnology has penetrated the market, the major impact will be at least a decade away. Currently, there are a few cosmetic products made by incorporating nanoparticles on the market. To create such macroscale materials, many

issues surrounding the incorporation of nanotubes into a matrix, strategies for property improvement, and the mechanisms responsible for those property improvements still remain critical. Since only a moderate success has been made over the last 20 years, researchers must continue to investigate strategies to optimize the fabrication of nanotube-enabled materials to achieve both improved mechanical and transport properties.

CHAPTER II

MATHEMATICAL DERIVATION AND NUMERICAL IMPLEMENTATION

As illustrated above, many important applications of polymer matrix composites (PMCs) reinforced by conductive fillers were found in aerospace and electronic industries. A common advantage of these composites is that certain material properties (thermal, electrical, mechanical or optical) are enhanced with minimum weight adding. It is of interest to investigate that how most optimized properties of the material can be reached by varying the geometry, orientation, length scale, distribution and volume fraction of the fillers. Conductive fibers are embedded in the polymer matrix in order to increase the overall conductivity of the composites. The overall conductivity of the composites is controlled by the volume fractions taken up by the fibers. However, the conductivity-volume fraction curve is not a simple smoothly upgoing one. Previous experimental study by Bigg D.M., 1979 [20] has revealed the existence of an insulator-to-conductor transition in such composites around a threshold as the volume fraction of the fibers reaches a critical value. It usually turns out to be a sharp onset of high conductivity *K* at a critical fiber volume fraction f_c (see Fig.2)

2.1 Percolation theory and Monte Carlo method

Percolation theory has been successful and widely accepted in describing this transition[21]. According to percolation theory, the conductive fillers can be modeled as a 2D or 3D network of numerous segments, which are located regularly or randomly within the system. The connections between each two neighboring segments may be

open with probability *p*, or closed (allowing the heat flow or current to go through) with the probability 1-*p*. It is found that there is a critical probability p_c above which a continuous pathway will always exist in the system. The studies on percolation of the composites have been focused on the investigation of the percolation threshold as to understand the change in conductivity near the insulator-conductor transition.

The exact solution to percolation problems have been obtained only for very few special cases [21], while the approximation methods, like Monte Carlo simulations, are expected to solve more general problems. The disordered topology is modeled with Monte Carlo method. The solution of the percolation process is obtained with the aid of computers with high computation capability.

The earliest application of Monte Carlo method to solve the percolation problem was conducted by Pike and Seager (1974) [22], who did a 2D study on composites filled with straight sticks. In their work, the sticks were assumed to be of the same fixed length and the size in width was ignored. Balberg and Binenbaum (1983) [23] extended Pike and Seager's study by accounting for the macroscopic anisotropy of the sticks' orientation, as well as the distribution of the stick's length. Natsuki (2005) [24] first considered the width of fibers in his Monte Carlo simulation for a 2D network. The dependence of percolation threshold on fibers' aspect ratio and orientation angles was investigated. Studies on 3D percolation problems were also present later, including Taya (1987) [25] and Lee (1995) [26]. The former studied the in-plane electrical conductivity of straight short fiber composites, while the latter predetermined the orientation angle of the fibers, and the randomness of the fiber distribution was highly violated.

It is understandable that the nanostrands in conductive composites take on high flexibility due to their extremely large length to diameter aspect ratios. The conductivity of such microstructure will certainly be different from that of the one which only contains straight fibers. To the date, the research on composites of fibers with different shapes has been done and much is still underway. For instance, Yi *et. al* (2004) [27] reported the increase of percolation threshold with the waviness of sinusoid-shaped fibers. Dalmas *et al* (2006) [28] simulated the 3D entangled fibrous network using a spline-shaped fiber model. However, the fibers diameter is not considered.

Most of the previous work focused on discussing electrical conductivity of the polymer composites. This is mainly due to the high sensitivity of the electrical conductivity to the percolation threshold. To the opposite, overall thermal conductivity of the polymer composites are less sensitive to the percolation threshold and becomes more difficult to predict quantitatively. In this work, a deeper insight into the effect of percolation threshold on the thermal conductivity will be discussed. Furthermore, the recent SEM image [29] of the real specimen of PMCs indicates that the fibers are not uniformly distributed anywhere in the polymer matrix, since the matrix consists of polymer emulsion particles and the fibers are only scattered along the particle surface (the interstitial area).

The algorithm of the Monte Carlo methods can be presented in two basic steps: 1. generating an appropriate percolation model; 2. imposing bonding criterion on two fibers for inter-fiber connections. At the first step, fibers with random orientations and random vertexes are generated. As our attention will be concentrated on the volume fraction at which the onset of high conductivity, a dimensionless system is more

convenient for us to carry out this study. We choose the length of the representative volume element (RVE) as the normalizing parameter so that the system of interest is modeled as a cube of unit lateral length. At the second step, the connectivity between each fiber pairs inside the RVE will be checked. Finally, the connected two or more fibers constitute a continuous cluster. The details of the implementation will be discussed later in the following sections.

2.2 Model generation

The model is set up in a Cartesian coordinate system. The continuum model of the carbon nanotube is a solid cylindrical stick (Fig. 3) which is assumed to be isotropic and homogeneous. In order to locate each fiber, we generate the random coordinates to the mid-point of the fiber. However, this is not enough to define the orientation of the fiber, so a local spherical system is induced to address this issue. The center of local coordinate system is set at the mid-point of the fiber. Two arms with half of the fiber length are defined. Diameter D is assigned to all the arms. Two independent angles α^i and θ^i are used to define the orientation of the arm (as shown in Fig. 4). Two angles are generated randomly and range from $[\mathbf{0},\pi]$ and $[\mathbf{0},\mathbf{2}\pi]$, respectively. Particularly, when the fiber *i* is straight, the angles of its two arms should satisfy $\alpha_{\mathbf{1}}^i + \alpha_{\mathbf{2}}^i = \pi$, and $\left|\theta_{\mathbf{1}}^i - \theta_{\mathbf{2}}^i\right| = \pi$. The fiber lengths of all the fibers in the system are taken to be identical. To generate numbers with sufficient randomness, the multiplicative congruential generator (MC generator) is adopted, which is the most common computation technique for producing random number sequences. The implementation details of this generator are given by Park and Miller (1988) [30]. To avoid the lattice effect (Anderson,1990)

[31], the MC generator is called once to generator the information needed for identifying the a fiber. That is, to generate six random numbers, and meanwhile the orientation angles are specified by the first three random numbers, and the orientation angles are specified by the other three random numbers which are entangled so that the angles are within proper ranges. As shown in Fig.5, two samples of filled by random array of 400 and 800 fibers are plotted.

2.3 Connection criteria

In the cube, the coordinates of the points on the axis of a fiber whose central point is located at (x_i, y_i, z_i) are given by as follows (shown in Fig. 6):

$$\begin{Bmatrix} x \\ y \\ z \end{Bmatrix} = \begin{Bmatrix} x_i \\ y_i \\ z_i \end{Bmatrix} + t \begin{Bmatrix} \cos\theta_1^i \sin\alpha_1^i \\ \sin\theta_1^i \sin\alpha_1^i \\ \cos\alpha_1^i \end{Bmatrix} \quad \text{or} \quad \begin{Bmatrix} x \\ y \\ z \end{Bmatrix} = \begin{Bmatrix} x_i \\ y_i \\ z_i \end{Bmatrix} + t \begin{Bmatrix} \cos\theta_2^i \sin\alpha_2^i \\ \sin\theta_2^i \sin\alpha_2^i \\ \cos\alpha_2^i \end{Bmatrix} \tag{1}$$

where (x_i, y_i, z_i) are the coordinates of the central point C; $t(\in [\mathbf{0}, L/\mathbf{2}])$ is the distance from C to the point of interest; $\alpha^i \in [\mathbf{0}, \pi]$ and $\theta^i \in [\mathbf{0}, \mathbf{2}\pi]$. There is a constraint among the orientation angles $\theta_1^i, \theta_2^i, \alpha_1^i$ and α_2^i, since the arm angle is predetermined (see Fig. 4). The constraint is

$$d = \mathbf{2}L \sin\frac{\gamma}{\mathbf{2}} \tag{2}$$

Here *d* is the distance between two end points of the angled fiber and it is a function of the orientation angles. By using Eq. (1) and (2) it can be expressed as:

$$\mathbf{1} - \cos\alpha_1^i \cos\alpha_2^i - \cos(\theta_1^i - \theta_2^i) \sin\alpha_1^i \sin\alpha_2^i = \mathbf{2}\sin^{\mathbf{2}}(\gamma/\mathbf{2}) \tag{3}$$

Only three of the four orientation angles $\left(\theta_1^i, \theta_2^i, \alpha_1^i, \alpha_2^i\right)$ are independent. Here α_1^i, α_2^i and θ_1^i are chosen to be independent parameters and to be generated by the random generator. θ_2^i can be expressed by Eq. (3).

The occurrence of the percolation in a given polymer matrix composite sample with conductive fillers has to be determined by computations. That is, the computation will identify whether there is a continuous conducting pathway along any one of or all the coordinate axes. The principle of the computation is as follows: Each fiber is checked against another to find whether they intersect. In this work, the connectivity between ith and jth fiber is determined by checking whether the minimum distance between their axes are greater than a critical value, typically the diameter of the fiber or even smaller. The shortest distance between two fibers can be found through the procedure below.

The line equations for the two axes can be expressed in a vector form as:

$$\begin{Bmatrix} x \\ y \\ z \end{Bmatrix} = \begin{Bmatrix} x_i \\ y_i \\ z_i \end{Bmatrix} + t \begin{Bmatrix} \cos\theta_m^i \sin\alpha_m^i \\ \sin\theta_m^i \sin\alpha_m^i \\ \cos\alpha_m^i \end{Bmatrix} \quad \text{or} \quad \begin{Bmatrix} x \\ y \\ z \end{Bmatrix} = \begin{Bmatrix} x_i \\ y_i \\ z_i \end{Bmatrix} + s \begin{Bmatrix} \cos\theta_n^i \sin\alpha_n^i \\ \sin\theta_n^i \sin\alpha_n^i \\ \cos\alpha_n^i \end{Bmatrix} \tag{4}$$

Here, s and t are, respectively, the relative distance to the central points of ith and jth fibers. The square of the distance between ant two points on the axes of the two fibers can be obtained from Eq. (4) as:

$$F = \mathbf{u} \cdot \mathbf{u} \tag{5}$$

where,

$$\begin{aligned} \mathbf{u} = (&x_i - x_j + t\cos\theta_m^i \sin\alpha_m^i - s\cos\theta_n^j \sin\alpha_n^j, y_i - y_j + t\sin\theta_m^i \sin\alpha_m^i \\ &- s\sin\theta_n^j \sin\alpha_n^j, z_i - z_j + t\cos\alpha_m^i - s\cos\alpha_n^j)^T \end{aligned} \tag{6}$$

Using Eq. (6) in Eq. (5), it gives:

$$F = t^2 + C_1 t + C_2 ts + s^2 + C_3 s + C_4 \tag{7}$$

where,

$$C_1 = \mathbf{2}\Delta x \cdot \sin\alpha_m^i \cdot \cos\theta_m^i + \mathbf{2}\Delta y \cdot \sin\alpha_m^i \sin\theta_m^i + \mathbf{2}\Delta z \cos\alpha_m^i \tag{8a}$$

$$C_2 = -\mathbf{2}\left[\sin\alpha_m^i \sin\alpha_n^j \cdot \cos\left(\theta_m^i - \theta_n^j\right) + \cos\alpha_m^i \cdot \cos\alpha_n^j\right] \tag{8b}$$

$$C_3 = -\mathbf{2}\Delta x \cdot \sin\alpha_n^j \cdot \cos\theta_n^j - \mathbf{2}\Delta y \cdot \sin\alpha_n^j \cdot \sin\theta_n^j - \mathbf{2}\Delta z \cdot \cos\alpha_n^j \tag{8c}$$

$$C_4 = \left(\Delta x\right)^2 + \left(\Delta y\right)^2 + \left(\Delta z\right)^2 \tag{8d}$$

$$\Delta x = x_i - x_{j\,j} \tag{8e}$$

$$\Delta y = y_i - y_j \tag{8f}$$

$$\Delta z = z_i - z \tag{8g}$$

From Eq. (7), it implies that F is a functions of two variables, s and t. To find its minimum value, it is necessary to differentiate Eq. (7):

$$\mathbf{0} = \frac{\partial F}{\partial t} = \mathbf{2}t + C_1 + C_2 s \tag{9a}$$

$$\mathbf{0} = \frac{\partial F}{\partial s} = \mathbf{2}s + C_3 + C \tag{9b}$$

Solving Eq. (9a,b), it is given:

$$\begin{cases} t_0 = \left(\mathbf{2}C_1 - C_2 C_3\right)/\left(C_2^2 - \mathbf{4}\right) \\ s_0 = \left(\mathbf{2}C_3 - C_1 C_2\right)/\left(C_2^2 - \mathbf{4}\right) \end{cases} \tag{10}$$

which defines the reflection point $\left(t_0, s_0\right)$. For $F(t_0, s_0)$ to be the minimum, it should hold that:

$$\mathbf{0} < \frac{\partial^2 F}{\partial t^2} \tag{11a}$$

$$\mathbf{0} < \frac{\partial^2 F}{\partial t^2} \cdot \frac{\partial^2 F}{\partial s^2} - \left[\frac{\partial^2 F}{\partial t \partial s}\right] \tag{11b}$$

From Eq. (7), it is followed by:

$$\frac{\partial^2 F}{\partial t^2} = \mathbf{2} > \mathbf{0} \tag{12a}$$

$$\frac{\partial^2 F}{\partial t^2} \cdot \frac{\partial^2 F}{\partial s^2} - \left[\frac{\partial^2 F}{\partial t \partial s}\right] = \mathbf{4} - C_2^2 > \mathbf{0} \tag{12b}$$

Eq. (12b) is always true as long as two fibers are not parallel to each other ($\alpha_i^m \neq a_j^n, \theta_i^m \neq \theta_j^n$), which means F has the minimum value when $t = t_0$ and $s = s_0$. Substituting Eq. (10) into Eq. (7), The minimum distance between the two fiber axes:

$$d_{\min} = \begin{cases} \left[\left(C_2^2 C_4 + C_1^2 + C_3^2 - C_1 C_2 C_3 - \mathbf{4} C_4\right) / \left(C_2^2 - \mathbf{4}\right)\right]^{1/2} at(t_0, s_0), if, \alpha_i^m \neq a_j^n, \theta_i^m \neq \theta_j^n \\ C_4 - c_1^2 / \mathbf{4}, at(s = C_1 / \mathbf{2}), if, \alpha_i^m = a_j^n, \theta_i^m = \theta_j^n \end{cases} \tag{13}$$

If the condition: $d_{\min} \leq D, \mathbf{0} \leq t_0 \leq L,$ and $\mathbf{0} \leq s_0 \leq L$ is satisfied, then two fibers connect. This connection is called body-to-body connection. (see Fig.7a). However, there are two special connection patterns in which two fibers do not satisfy the above condition but still connect: the end-to-body and end-to-end connections (see Fig.7b and Fig.7c). For the end-to-body connection, the connection criterion is the distance between the end circle of one fiber and the central line of another fiber is smaller or equal to D. Similarly, for the end-to-end connection, the connection criterion is that the distance between the end circles of two fibers is no larger than D. The end circle of a fiber will be discretized as several points during the computer implementation. Here, note that $d_{\min} \leq D$ is the necessary condition for all patterns of connections. Also, if the intersection point of two fibers is outside the sample boundaries, they will not be considered to be intersected.

The last two end connection patterns are much more time-consuming in computation. We estimate their quantitative effect by calculating the percentage of the end connections in the whole connections among fibers in the model. It is found that the percentage decreases dramatically with the increase of the fiber aspect ratio. The

percentage is 6% as the aspect ratio reaches 24. Simulation with and without the end connections taken into account are performed for fiber with aspect ratio 24. The difference in the results is negligible. Therefore, for computation efficiency, the end connections are ignored for fibers with aspect ratio higher than 24.

2.4 Computer code implementation

The Fortran 90 computer code is implemented on Linux system supported by the supercomputing facility Cosmos at Texas A&M University. The model is set up within a cubic space with unit length (scaled by the real thickness of the polymer matrix composites). In other words, it is non-dimensional. The purpose of scaling is to simplify the data processing especially when extracting the results of the calculation.

The first step is to generate the fibers and fill them into the model, which are of the same fiber length and aspect ratio (fiber length divided by fiber diameter). Each fiber is characterized by five independent parameters: coordinates of the fiber geometry center (x,y,z); two angles θ and α . Furthermore, since the fiber length is predetermined, the coordinates of two fiber ends can be calculated. Since the fibers are randomly distributed and oriented in the model, five parameters x, y, z, θ and α are supposed to be random numbers within certain ranges: $x, y, z \in [\mathbf{0},\mathbf{1}]$; $\theta \in [\mathbf{0},\mathbf{2}\pi]$ and $\alpha \in [\mathbf{0}, \pi]$, respectively. Different random number generators were developed, and they basically should have the following features: firstly, being capable of produce uncorrelated number sequence; secondly, having a long period (in case of the repetition of sequences); thirdly, being capable of produce a uniformly distributed number series; finally, high efficiency.

In this study, we select a commonly accepted random number generator, which represents one of the oldest and best-known pseudorandom number generator algorithms. The generator produces a sequence of numbers by using equations of the form:

$$S_i = AS_{i-1} + C \bmod m, \tag{14}$$

where S_i is the ith random number seed generated; A is some multiplier; m is a modulus and C is some constant. There are rules and tests that help choosing good values of A, C and m, for instance, to ensure that the parameters are chosen so they give full period. This algorithm is particularly important for Monte Carlo methods due to its reliance on random sampling computation. Meanwhile, each fiber is assigned a fiber number and a cluster number. Initially, fiber numbers are sequentially assigned to each fiber from 1 to N, which is the total number of the fibers and the cluster number is set to be equal to the fiber number. In Fig. 8, the random distribution of azimuthal angles for 400 fibers is shown.

Next, it is necessary to count the fiber number on the upper and lower boundaries. Two arrays are defined to store the upper and lower boundary fiber numbers. Then a subroutine is called to check the connectivity of fibers. Each fiber is checked against all the other fibers whose fiber numbers are higher. For example, the ith fiber will be checked with the fibers with fiber number form i+1 through N. The connectivity criterion is defined in two steps. Firstly, it must be true that two fibers i and j have overlapping in all three coordinate directions and therefore, the following condition has to be satisfied:

$$x_{\min}^{j} > x_{\max}^{i} \text{ or } x_{\max}^{j} < x_{\min}^{i}$$

$$y^{j}_{\min} > y^{i}_{\max} \text{ or } y^{j}_{\max} < y^{i}_{\min}$$

$$z^{j}_{\min} > z^{i}_{\max} \text{ or } z^{j}_{\max} < z^{i}_{\min}$$

If all the conditions above are not satisfied, the two fibers *i* and *j* are not possible to intersect, then fiber *i* will be checked against the next fiber *j*+1. If they are satisfied, the distance between two fibers is calculated using the expression in Eq. (13). The result will be compared to the value of the diameter of the fibers. If larger than the diameter, two fibers do not intersect. If smaller or equal to the diameter, it can be regarded that two fibers intersect. The smaller distance than the diameter is possible, because some of the connected fibers are soldered by using microwave in the manufacturing process. If a fiber pair meets the above criterion, their cluster numbers will be set the smaller one of the two original cluster numbers. This has to be done to make sure all the fibers in the same cluster have the same cluster identification number. Also two clusters are marked with the same number if they share one or more common fibers. The fiber numbers of all the fibers in a cluster will be compared to the boundary fiber number stored in two arrays defined above. If both upper and lower boundary fibers are found in the same cluster, it can be concluded that two boundaries are connected and the sample is percolated in the direction perpendicular to the opposite boundaries, as shown in Fig. 9. The critical volume fraction (CVF) is defined as the instantaneous volume fraction of the fibers when the percolation happens for the very first time in the system.

CHAPTER III

RESULTS AND DISCUSSION

One of the purposes of the numerical simulations is to investigate the filler's size effect on the percolation threshold. In other words, the effects of fiber length and aspect ratio on the critical volume fraction will be studied. For better accuracy of the results, the calculation on each sample will be performed 10 times, as shown in Table 1, and the standard deviation will be evaluated so that the abnormal results (maximum and minimum values) will be used to create an error bar on each data point. Then the average of the rest values will be calculated and used as the critical volume fraction. Here below is an example:

Table 1
Calculated results (10 repetitions) of critical volume fraction of fibers in the cube of unit length in which fiber length = 0.080; aspect ratio = 26.7; fiber diameter = 0.003

Total Fiber Number	Critical Volume Fraction	Number of Clusters
10500	0.0059	1
10600	0.006	1
10700	0.0061	1
10200	0.0058	1
11000	0.0062	1
10400	0.0059	1
9300	0.0053	2
11100	0.0063	1
10600	0.006	1
11000	0.0062	1

As shown above, within a sample RVE (a cube of unit length), fibers of length 0.08 and aspect ratio 26.7 are distributed randomly. The initial fiber number is set to be 500 for this case. Then the computation will do a search over the system to find the fiber cluster of percolation. Once such a cluster is found, the cluster number will be set to 1 (initially 0) and the computation will be terminated. The current volume fraction will be regarded as the critical volume fraction of the system. If the cluster number is still zero after a search, a small increment (100 for this case) will be added to the fiber number and the computation will repeated. A enough large upper bound of fiber number will be set to terminate the calculation when it takes too long. Such a situation will be regarded as an convergency problem. The initial fiber number, the increment and the upper bound will be adjusted based on the dimension of the fibers. It is important that the cluster number is 1, because it makes sure that the simulation is at the first time two opposite boundaries are connected by fibers. By calculating the standard deviation of 10 repetitions, the stability of the results is evaluated. Here the standard deviation equals to 521.1099 and the error (standard deviation divided by average fiber number) equals to 4.94%, which is within the tolerance (5%). It is also observed that abnormal cases could take place in the cases of maximum or minimum fiber numbers. For example, in the row 7 of Table 1, the result has a considerable discrepancy comparing to the results in other rows. Also, the cluster number is larger than 1. It implies that the percolation was obtained much easier and faster and this result cannot represent the general case. To make the results more accurate, the maximum and minimum values are picked out and the average is calculated for the rest rows and is considered to be the final result.

3.1 Effect of the fiber length

In the Monte Carlo simulations, the finite-size effect must be taken into account. Based on the definition, the percolation threshold happens at the moment when an infinitely large cluster is found in the system. However, it is unrealistic to model an infinite system in the numerical simulation, but it is a good possibility to use the extrapolated results from Monte Carlo simulations to predict the thresholds for an infinite system. Stauffer [21] revealed the relationship between percolation threshold P_c for finite-size system and P_∞ for infinite system, which is expressed as:

$$P_c - P_\infty \propto C^{-1/\nu} \tag{15}$$

where C is called the characteristic size of the simulation; ν is the correlation length exponent. In this work, as described in the foregoing sections, the fibers are embedded in a cubic box of unit length ($x \in [\mathbf{0},\mathbf{1}], y \in [\mathbf{0},\mathbf{1}], z \in [\mathbf{0},\mathbf{1}]$). Since the size of the fiber is normalized by the actual size of the system (usually $\mathbf{25} \sim \mathbf{50}\mu m$), it is concluded that the normalized fiber length is inversely proportional to the system size and from (14):

$$P_c - P_\infty \propto L^{1/\nu} \tag{16}$$

According to such a relation, it is reasonable to predict that the critical volume fraction is a power law function of the normalized fiber length. By fitting the curve of the numerical results, ν can be figured out easily. The next step is to extrapolate the critical volume fraction versa $L^{1/\nu}$, the plotted results are supposed to follow a straight line (linear relationship). Intersection point between the straight line and the Y-axis represents the critical volume fraction for an infinitely large system. In this study, a wide range of diameter sizes are selected: (0.005, 0.008, 0.010, 0.012, 0.014); for each fixed diameter size, critical volume fractions for samples with fiber lengths 0.08, 0.10,

0.14, 0.16, 0.18, 0.20 and 0.24 are calculated. Fig. 10 indicates the trend line of the plotted results of the critical volume fraction to the normalized fiber length. Functions of power law are used in the curve fitting Fig. 11. Due to the non-linearity it is difficult to use the power-law functions to predict the critical volume fraction accurately. As listed in Table 2., the intersection points are found, however, it is meaningless since it represent samples with cube length to be zero. The linearization is unsuccessful here.

Table 2
Calculated results from the curve fitting

Fiber Diameter	ν	$-1/\nu$	Intersection Point
0.005	0.790888959	-1.2644	0.004
0.008	0.865276456	-1.1557	0.0018
0.010	0.888651915	-1.1253	0.0006
0.012	0.985027581	-1.0152	0.00007
0.014	1.044713748	-0.9572	0.00001

In Fig. 10, it is found that the critical volume fraction decreases when the fiber length increases. The critical volume fraction depends on two factors, the single fiber dimensions and the total fiber number at the percolation threshold. It is understandable that the probability that two randomly distributed fibers connect is larger

when their length increases. However, smaller fibers have more difficulty to be connected and percolation happens at larger number of fibers. Tables 3-5 show the calculated total fiber numbers at the moment of percolation threshold. Meanwhile, it is concluded that the critical volume fraction increases with the fiber diameter when the fiber length keeps unchanged.

Table 3
Calculated fiber numbers for sample with fiber diameter D=0.005

Repetition	L=0.08	L=0.10	L=0.14	L=0.16	L=0.18	L=0.20	L=0.24
1	11000	7200	3200	2800	1700	1100	1000
2	9500	6400	3200	2600	2200	1300	1000
3	10900	7100	3300	2700	1800	1500	800
4	12000	7300	3400	2500	2000	1700	1000
5	11100	6700	3100	2300	1600	1500	1000
6	10900	6300	3400	1800	1700	1200	700
7	11000	7400	2900	2700	1800	1600	800
8	12100	7300	3300	2600	2100	1100	1000
9	10300	6400	3700	2600	1600	1300	800
10	9800	6800	3700	2700	1800	1400	900

Table 4
Calculated fiber numbers for sample with fiber diameter D=0.010

Repetition	L=0.08	L=0.10	L=0.14	L=0.16	L=0.18	L=0.20	L=0.24
1	7400	4400	2500	1800	1000	1000	600
2	6200	3900	2400	1500	1200	1000	700
3	7000	4400	2400	1700	1400	1200	700
4	7000	4700	1900	2000	1500	900	600
5	6900	4400	2400	1300	1200	900	900
6	6600	3800	2300	1600	1500	1000	600
7	6500	4500	2400	1800	1000	900	500
8	7300	4100	2200	1400	1100	1000	600
9	6400	4600	2500	1400	1000	1200	800
10	7400	4200	2400	1500	1400	1000	700

Table 5
Calculated fiber numbers for sample with fiber diameter D=0.016

Repetition	L=0.08	L=0.10	L=0.14	L=0.16	L=0.18	L=0.20	L=0.24
1	5600	3900	2100	1500	1300	800	700
2	5500	3300	2200	1400	1300	1100	700
3	5800	3300	1600	1200	1100	800	700
4	4400	4100	2000	1400	1000	900	700
5	5400	4100	2100	1400	1200	700	600
6	5800	3400	1700	1500	1000	900	600
7	5600	3800	1600	1400	1300	1100	600
8	5900	3700	1600	1500	1200	1000	600
9	5600	3600	1800	1500	1200	800	700
10	5500	3400	1900	1400	1100	900	700

The results in Tables 3-5 imply that the fiber number is the dominant factor in the change of CVF, since from Fig. 10, it is concluded that the CVF decreases with the increasing fiber length.

3.2 Effect of the aspect ratio

Aspect ratio is another very important factor which affects the percolation threshold. In this study, a set of fiber lengths are selected and for each fiber length several samples of different aspect ratio are used to calculate the critical volume fractions, f_c. The results are plotted in Fig. 11.: the critical volume fractions f_c decreases dramatically with the increasing aspect ratio, which means the critical volume fraction decreases with the decreasing fiber diameters. The volume of a single fiber is proportional to the square of the fiber diameter and the fiber number needed for percolation threshold increases when the fibers become thinner, because it is more difficult to get a fiber pair connected. As discussed in the foregoing section, the fiber number is the dominant factor in determining the critical volume fraction when the fiber length changes. To the contrary, the single fiber volume affects the critical volume fraction to a larger extent when fiber diameter changes. The results in Fig. 18 coincide with the conclusion form the previous experimental study by D. Bigg (1979) [20]: the percolation threshold relies on the aspect ratio greatly in the case of short fiber reinforced composites, that is, the higher the fiber aspect ratio is, the lower the volume fraction is demanded to obtain conductance. However, the simply plotted results are still ambiguous to predict the trend between critical volume fraction and aspect ratio. Natsuki's research work in 2005 [24] revealed that the logarithm of the critical volume

fraction has a linear dependence on that of the aspect ratio of the fibers. Here logarithms of the results are also calculated as shown in Table 6.

Table 6
Logarithms of aspect ratios and critical volume fractions (L=0.08)

Aspect ratio (AR)	CVF (f_c)	ln (AR)	ln(f_c)
5.7	0.068963	1.740466	-2.67419
6.7	0.05475	1.902108	-2.90498
8	0.043288	2.079442	-3.13989
10	0.03295	2.302585	-3.41276
16	0.017075	2.772589	-4.07014

Table 7
Logarithms of aspect ratios and critical volume fractions (L=0.10)

Aspect ratio (AR)	CVF (f_c)	ln (AR)	ln(f_c)
7.1	0.056175	1.960095	-2.87928
8.3	0.0448	2.116256	-3.10555
10	0.033875	2.302585	-3.38508
12.5	0.02605	2.525729	-3.64774
20	0.01355	2.995732	-4.30137

Table 8
Logarithms of aspect ratios and critical volume fractions (L=0.14)

Aspect ratio (AR)	CVF (f_c)	ln (AR)	ln(f_c)
10	0.039875	2.302585	-3.22201
11.7	0.0307	2.459589	-3.48349
14	0.026125	2.639057	-3.64486
17.5	0.017513	2.862201	-4.04484
28	0.009138	3.332205	-4.69537

Table 9
Logarithms of aspect ratios and critical volume fractions (L=0.16)

Aspect ratio (AR)	CVF (f_c)	ln (AR)	ln(f_c)
11.4	0.0354	2.433613	-3.34104
13.3	0.026663	2.587764	-3.6245
16	0.019938	2.772589	-3.91515
20	0.0149	2.995732	-4.20639
32	0.00815	3.465736	-4.80974

Table 10
Logarithms of aspect ratios and critical volume fractions (L=0.18)

Aspect ratio (AR)	CVF (f_c)	ln (AR)	ln(f_c)
12.9	0.032575	2.557227	-3.42421
15	0.025463	2.70805	-3.67055
18	0.017325	2.890372	-4.0556
22.5	0.013375	3.113515	-4.31437
36	0.006425	3.583519	-5.04756

Table 11
Logarithms of aspect ratios and critical volume fractions (L=0.20)

Aspect ratio (AR)	CVF (f_c)	ln (AR)	ln(f_c)
14.3	0.0277	2.66026	-3.58632
16.7	0.021488	2.815409	-3.84028
20	0.015688	2.995732	-4.15489
25	0.0116	3.218876	-4.45675
40	0.00535	3.688879	-5.23066

Table 12
Logarithms of aspect ratios and critical volume fractions (L=0.24)

Aspect ratio (AR)	CVF (f_c)	ln (AR)	ln(f_c)
17.1	0.024513	2.839078	-3.70857
20	0.017988	2.995732	-4.01808
24	0.012488	3.178054	-4.38303
30	0.009213	3.401197	-4.68719
48	0.0043	3.871201	-5.44914

Fig. 12 is the plotted results in Tables 7-12. It indicates that the linear relationship between the natural logarithm of fiber aspect ratio AR and critical volume fraction $f_{c.}$ The slopes of the straight line in Fig. 12 are the coefficients of the linear functions of curve fitting. The slopes varies with the fiber length a little bit, but it is around -1.40 on average (Fig. 14). This means that the critical volume fraction is generally proportional to AR-1.40. The result is twice as that of Bigg's experimental

data [20] but closer to Foygel's theoretical and computational studies of carbon nanotube composites in 2005 [32].

Samples filled with low-aspect ratio fibers are more difficult to reach the percolation threshold because critical volume fraction can be much higher than that for high-aspect ratio fibers. The computation becomes also much more time-consuming and even fails as a result of inconvergency. It is unrealistic to perform calculations on all the samples. The success of linearization makes it possible to predict the critical volume fractions of low-aspect ratio fibers more accurately than directly using curve-fitting results, which follows the power law and is non-linear. Furthermore, the intersecting point between the linear function and the y-axis represents the logarithm of the critical volume fraction when the fiber length equals to the diameter, in other words, the fillers become particles, not fibers any more.

3.3 Effect of the emulsion particle size

In the above sections, the nano-fibers are assumed to randomly located anywhere in the samples. The polymer matrix is considered to be homogeneous and isotropic. However, such a spatial distribution of fibers is not realistic in practice. For instance, the polymer matrix is fabricated from poly(vinyl acetate) (PVAc) homopolymer emulsion (Vinac XX210) (Air Products, Inc.), which consists of polymer particles and water. When the fibers are scattered in the emulsion, they cannot penetrate the particles. After the water is drained, most volume is taken up by the polymer particles and the fiber are accommodated in the interstitial space between the particles.

To model the real microstructure of the polymer composites, it is necessary to exclude the fibers from the volume of particles. This requires check the locations of fibers after N random fibers are generated. Suppose there are N' fibers are located in the particles. Then they will be removed and the rest $N - N'$ fibers are kept. A new set of N' random fibers are regenerated. This process will be repeated till N fibers are placed in the interstitial spaces. The topology of particles in the real microstructure can be described using Voronoi tessellation (Fig. 15), however, it will be computationally troublesome, so in the simulation, all particles are assumed to be cubes with identical length for simplicity and the width of the interstitial space is set to be 10% of the particle size. Particles of different sizes are used.

Similarly, the effects of the fiber size on the critical volume fractions will be investigated and compared to those results in the foregoing sections. The fiber diameter is selected to be 0.003, 0.005 and 0.010 respectively. The results are plotted in Fig. 16-18. It is found that the critical volume fractions decrease compared to that of samples without particles given the same fiber length and diameter. Also when the normalized particle size increases, the critical volume fraction decreases. This is understandable since the existence of the particles narrows the volume for accommodating the nano-fibers and the probability of fiber connections are larger. The curve fitting is made by adding a trend line (dash line) to the calculated results (dots). It is noticed that the power law still works well. The critical volume fraction decreases with the increasing fiber length. The normalized fiber lengths (0.005~0.014) used are smaller that that in the previous sections because it does not make good sense that the fiber length is larger than the polymer particle size.

3.4 Electrical and thermal conductivity

According to B.I. Shklovskii and Al.L. Efros [33] and D. Stauffer [21], electrical conductivity of nano-fiber network composites after the percolation threshold is expressed in Eq. (15):

$$\sigma_c = \sigma_o \left(f - f_c \right)^t \tag{17}$$

where σ_c is the overall electrical conductivity of the polymer composites; σ_o is the pre-exponential coefficient that is usually equal to the conductive phase (nano-fiber here); f_c is the critical volume fraction and f is the volume fraction; t is the conductive exponent. This power law expression has been validated analytically (D. Stauffer, 1985 [21]) and experimentally (Y. Hernandez et al. 2007 [34] , C. Yu and J. Granlan [29]). The exponent *t* is regarded as a universal value for two-phase composites. According to C. Yu and J. Granlan [29], here the value of *t* is set to be 3.44 and σ_o equals to 1.26×10^6 S/m. Then calculated volume fractions in the previous sections are inserted into Eq. (17) and plotted the results in Fig. 19 and 20. The plotted results show that the electrical conductivity increases with the fiber length. And also the conductivity curves of samples with particles are above those of samples without particles. It is concluded that the larger electrical conductivities also attributes to the addition of particles. Fig. 21 shows the logarithm plotting of the electrical conductivity, which also increases with the volume fraction. It is of interests to find that the curves become parallel to the Y-axis when it approaches to the zero point. The offset between the curve and Y-axis is equal to the critical volume fraction. This indicates that the at the percolation threshold there is a sharp increase in the electrical conductivity.

The power law succeeds in predicting the electrical conductivity after percolation threshold. However, experimental results imply that the thermal conductivity does not increase so dramatically as electrical conductivity. This is due to the insensitivity of thermal conductivity to the fiber connection. Although the conductivity of the polymer composites depends on the volume fraction of the conductive fillers, the contact area needs to be taken into account. Heat flow will be hard to go through if the connection between fibers is weak. The quantitative study of thermal conductivity of composite materials are carried out by L.E. Nielsen (1974) [35]. This study accounts for the filler's geometry, matrix and filler properties and the volume loading of the filler:

$$\frac{K_c}{K_p} = \frac{\mathbf{1} + ABf}{\mathbf{1} - B\psi f} \tag{18}$$

where K_c is the overall thermal conductivity of the polymer composites, K_p is the thermal conductivity of the polymer, which can be very low; f is the volume fraction of the fillers. *B* is defined as:

$$B = \frac{K_f / K_p - \mathbf{1}}{K_f / K_p + A} \tag{19}$$

where K_f is the thermal conductivity of the filler. *A* is a geometrical term depending on the particle shape, aspect ratio and /or degree of aggregation. Value A is given in [35]. ψ is defined as:

$$\psi = \mathbf{1} + \left[\frac{\mathbf{1} - \phi_m}{\phi_m^2} \right] f \tag{20}$$

where ϕ_m is the maximum packing fraction of the filler. This term is determined experimentally for the best. Tables 13 and 14 give the values of *A* and ϕ_m :

Table 13
Maximum packing fraction ϕ_m [35]

Shape of Particle	Type of Packing	ϕ_m :
Spheres	Hexagonal close	0.7405
Spheres	Face centered cubic	0.7405
Spheres	Body centered cubic	0.60
Spheres	Simple cubic	0.524
Spheres	Random close	0.637
Spheres	Random loose	0.601
Rods or fibers	Uniaxial hexagonal close	0.907
Rods or fibers	Uniaxial simple cubic	0.785
Rods or fibers	Uniaxial random	0.82
Rods or fibers	Three dimensional random	0.52

Table 14
Value of A for various two-phase systems [35]

Type of dispersed phase	Direction of Heat flow	*A*
Spheres	Any	1.50
Aggregates of spheres	Any	2.50
Randomly oriented rods AR = 2.0	Any	1.58
Randomly oriented rods AR = 4.0	Any	2.08
Randomly oriented rods AR = 6.0	Any	2.80
Randomly oriented rods AR = 10.0	Any	4.93
Randomly oriented rods AR = 15.0	Any	8.38

Nielsen's formula considers the fillers as a random distribution and orientation in the space. The geometry of the fillers is also taken into account, so the theory can be applied to a wide range of systems including particle reinforced composites and fiber reinforced composites. However, this theory does not provide a solution to other kinds of spatial distribution patterns such as gradient distributions or clustered distributions. The clustered distribution will definitely increase the conductivity of the composites. For instance, when the fibers are connected in a chain, the heat flow will go through the medium more easily. Based on Nielsen's theory, the thermal conductivity will go up steadily with the increasing volume fraction of the conductive fibers. This result does not match the experimental data. The reason of such a deviation is that the when the volume fraction increases, the distribution pattern may change. At the turning point of such a change in the microstructure, there will be a jump

in the thermal conductivity. Take the percolation threshold for example, the total volume fraction of the fibers can be now split into two parts: the volume fraction of disconnected fibers and volume fraction of connected fiber in the percolation cluster:

$$f_f = f_{con} + f_{dis} \tag{21}$$

where f_f is the total volume fraction of the fibers; f_{con} is the volume fraction in the percolation cluster and f_{dis} is the volume fraction of the disconnected fibers.

Now it is obvious that the volume fraction used in Nielsen's formula should be f_{dis}. f_f is the term will contribute to the sudden increase in the thermal conductivity. Consider a extreme case where all the fibers are connected and aligned parallel through the polymer matrix Fig. 22, an equivalent model is polymer matrix with long parallel cylindrical fibers going through it. The thermal conductivity of this model can be then expressed as:

$$K_c = f_f K_f + f_p K_p \tag{22}$$

Now Eq. (18) and (22) are plotted in Fig. 22: the red line represents Eq. (22) and the purple line represents Eq. (18), Nielsen's formula. It is observed that the thermal conductivity calculated by using Eq. (22) increases much faster than that calculated by using Eq. (18). These two extreme situations can be considered as upper and lower boundaries of the real thermal conductivity of the composites. At the percolation threshold, the thermal conductivity should be a combination of both Eq. (18) and (22):

$$K_c = \left(f_{con} K_f + f_p K_p\right) + \frac{\mathbf{1} + AB f_{dis}}{\mathbf{1} - B\psi f_{dis}} K_p \tag{23}$$

After the moment of percolation threshold, the volume fraction of connected fibers keeps unchanged so that the first term in Eq. (23) does not change either. The increased

volume fraction of the fibers will be added to f_{dis} till next percolation chain is found in the system. So the slope of the thermal conductivity equals to that of Nielsen's formula. The complete expression for the thermal conductivity is:

$$K_c = \begin{cases} \dfrac{1 + ABf_f}{1 - B\psi f_f} K_p, f_f < f_c \\ f_{con} K_f + f_p K_p + \dfrac{1 + ABf_{dis}}{1 - B\psi f_{dis}} K_p, f_f \geq f_c \end{cases} \quad (24)$$

f_{con} Increases at each percolation point and the plotting of Eq. (24) will be upward stairs. This explains why the thermal conductivity of the composites is less sensitive to the first percolation threshold than electrical conductivity: the thermal conductivity is related to the cross section area of the conductive pathway, while electrical conductivity does not, so the thermal conductivity increases gradually and the electrical conductivity could present a sharp climb at the percolation threshold.

The results of actual thermal conductivity of composites containing fibers of diameter 0.005 and fiber length 0.08 are plotted in Fig 23. The solid blue line has the same slope as the purple line and will jump up at the next moment when percolation pathway is found. However, the current algorithm is only designed to find the percolation threshold and will terminate the simulation afterwards. Therefore, in the future work, the attention will be paid to find multiple percolation pathways.

CHAPTER IV

SUMMARY AND CONCLUSIONS

In this study, mathematical model is set up for a cubic nano-fiber network polymer matrix composites sample of unity length. The fibers are considered as line segments in a spherical coordinate system. Monte Carlo method is then used to generate the model by fill the randomly distributed and orientated fibers into the cube. The fibers are located by assigning random numbers between 0 and 1 to the coordinates of the fiber center point. Connection criterion is used to judge the connectivity of each fiber and its neighbors. Critical volume fractions are calculated for different fiber lengths and aspect ratios. Power-law function is used to predict the electrical conductivity after the percolation threshold. The thermal conductivity is studied by using combining Nielsen's theory and the commonly used empirical formula. Initial efforts are made to explain the insensitivity of the thermal conductivity to the percolation threshold. In the future, more work needs to be done to predict the thermal conductivity more accurately.

REFERENCES

[1] Iijima S. Helical microtubules of graphitic carbon, Nature 1991; 354(6348): 56.

[2] Iijima S, Ichihashi T. Single-shell carbon nanotubes of 1-nm diameter, Nature 1993; 363(6430): 603–605.

[3] Bower C, Rosen R, Jin L, Han J, Zhou O. Deformation of carbon nanotubes in nanotube-polymer composites, Applied Physics Letters 1999; 74(22): 3317–3319.

[4] Cooper CA, Ravich D, Lips D, Mayer J, Wagner HD. Distribution and alignment of carbon nanotubes and nanofibrils in a polymer matrix, Composites Science and Technology 2002; 62(7–8): 1105–1112.

[5] Haggenmueller R, Gommans HH, Rinzler AG, Fischer JE, Winey KI. Aligned single-wall carbon nanotubes in composites by melt processing methods, Chemical Physics Letters 2000; 330(3–4): 219–225.

[6] Jin L, Bower C, Zhou O. Alignment of carbon nanotubes in a polymer matrix by mechanical stretching, Applied Physics Letters 1998; 73(9): 1197–1199.

[7] Jin Z, Pramoda KP, Xu G, Goh SH. Dynamic mechanical behavior of meltprocessed multi-walled carbon nanotube/Poly (methyl methacrylate) composites, Chemical Physics Letters 2001; 337(1–3): 43–47.

[8] Kearns JC, Shambaugh RL. Polypropylene fibers reinforced with carbon nanotubes. Journal of Applied Polymer Science 2002; 86(8): 2079–2084.

[9] Lozano K, Barrera EV, Nanofiber-reinforced thermoplastic composites. Thermo analytical and mechanical analyses. Journal of Applied Polymer Science 2001; 79(1): 125–133.

[10] Potschke P, Fornes TD, Paul DR. Rheological behavior of multiwalled carbon nanotube/polycarbonate composites. Polymer 2002; 43(11): 3247–3255.

[11] Safadi B, Andrews R, Grulke EA. Multiwalled carbon nanotube polymer composites: synthesis and characterization of thin films. Journal of Applied Polymer Science 2002; 84(14): 2660–2669.

[12] Schadler LS, Giannaris SC, Ajayan PM. Load transfer in carbon nanotube epoxy composites. Applied Physics Letters 1998; 73(26): 3842–3844.

[13] Lau KT, Hui D. The revolutionary creation of new advanced materials carbon nanotube composites. Composites Part B 2002; 33: 263.

[14] Fielding JC, Chen C, Borges J. Vacuum infusion process for nanomodified aerospace epoxy resins, In: SAMPE Symposium & Exhibition, Long Beach, CA.

2004

[15] Hussain F, Derrick D, Haque A, Shamsuzzoha AM. S2 glass/vinyl ester polymer nanocomposites: manufacturing, structures, thermal and mechanical properties. Journal of Advanced Materials 2005; 37(1): 16–27.

[16] Haque A, Hussain F, Derrick D, Shamsuzzoha AM. S2 glass/epoxy polymer nanocomposites: manufacturing, structures, thermal and mechanical properties. Journal of Composites Materials 2003; 37(20): 1821–1837.

[17] Chowdhury FH, Hosur MV, Jeelani S. Studies on the flexural and thermomechanical properties of woven carbon/nanoclay-epoxy laminates. Materials Science and Engineering A 2006; 421: 298–306.

[18] Roy S, Hussain F, Lu H, Narasimhan K. Characterization and modeling of strength enhancement mechanism in polymer clay nanocomposites, In: AIAA Conference Proceedings, Austin. 2005.

[19] Roy S, Hussain F, Vengadassalam K, Lu H. Manufacturing, mechanical characterization, and modeling of a pultruded thermoplastic nanocomposite. In Nanoengineering of structural, functional and smart materials, 1st ed. edited by Schulz MJ, Kelkar AD, Sundaresan MJ. Taylor & Francis; USA, 2006.

[20] Bigg DM. Mechanical, thermal, and electrical properties of metal fiber-filled polymer composites. Polymer Engineering and Science 1979; 19(16): 1188-1192.

[21] Stauffer D. 2nd ed. Introduction of percolation theory, Taylor and Francis; London 1992.

[22] Pike GE, Seager CH. Percolation and conductivity - computer study .I. Physical Review B 1974; 10:1421-1434.

[23] Balberg I, Binenbaum N, Anderson CH. Critical behavior of the two-dimensional sticks system. Physical Review Letters 1983; 51: 1605 – 1608.

[24] Natsuki T, Endo M, Takahashi N. Percolation study of orientated short-fiber composites by a continuum model. Physica A 2005; 352:498-508.

[25] Taya, M. and Ueda, N. Prediction of the in-plane electrical conductivity of a misoriented short fiber composite: fiber percolation model versus effective medium theory. Journal of Engineering Materials and Technology 1987; 109: 252–256.

[26] Lee YH. Three-dimensional electrical percolation behavior in conductive short-fibre composites. Journal of Materials Science 1995; 30: 3033-3036.

[27] Yi YB, Berhan L, Satry AM. Statistical geometry of random fibrous networks, revisited: waviness, dimensionality, and percolation. Journal of Applied Physics

2004; 96: 1318-1327.

[28] Dalmas F, Dendievel R, Chazeau L, Cavaille JY, Gauthier C, Carbon nanotube-filled polymer composites. Numerical simulation of electrical conductivity in three-dimensional entangled fibrous networks, Acta Materialia 2006, 54: 2923-2931.

[29] Yu C, Kim YS, Kim D, Grunlan J. Thermoelectric behavior of segregated-network polymer nanocomposites. Nano Letters 2008; (in press)

[30] Park SK, Miller KW. Random number generators: good ones are hard to find. Communications of the ACM 1988; 1192-1201.

[31] Anderson SL. Random number generators on vector supercomputers and other advanced architectures. SIAM Review 1990; 32: 221-251.

[32] Foygel M, Morris RD, Anez D, French S, Sobolev VL. Theoretical and computational studies of carbon nanotube composites and suspensions: electrical and thermal conductivity. Physical Review B 2005; 71:104201.

[33] Sur A, Lebowitz JL, Marro J, Kalos MH, Kirkpatrick S. Monte Carlo studies of percolation phenomena for a simple cubic lattice. Journal of Statistical Physics 1976; 15:345-353.

[34] Hernandez YR, Gryson A, Blighe FM, Cadek M, Nicolosi V, Blau YJ, Gun'ko Y, Coleman JN. Comparison of carbon nanotubes and nanodisks as percolative fillers in electrically conductive composites. Scripta Materialia 2008; 58: 69-72.

[35] Nielsen LE. The electrical and thermal conductivity of two-phase systems. Industrial and Engineering Chemistry Fundamentals 1973; 13(1): 17–20.

APPENDICES

APPENDIX A

THE FIGURES

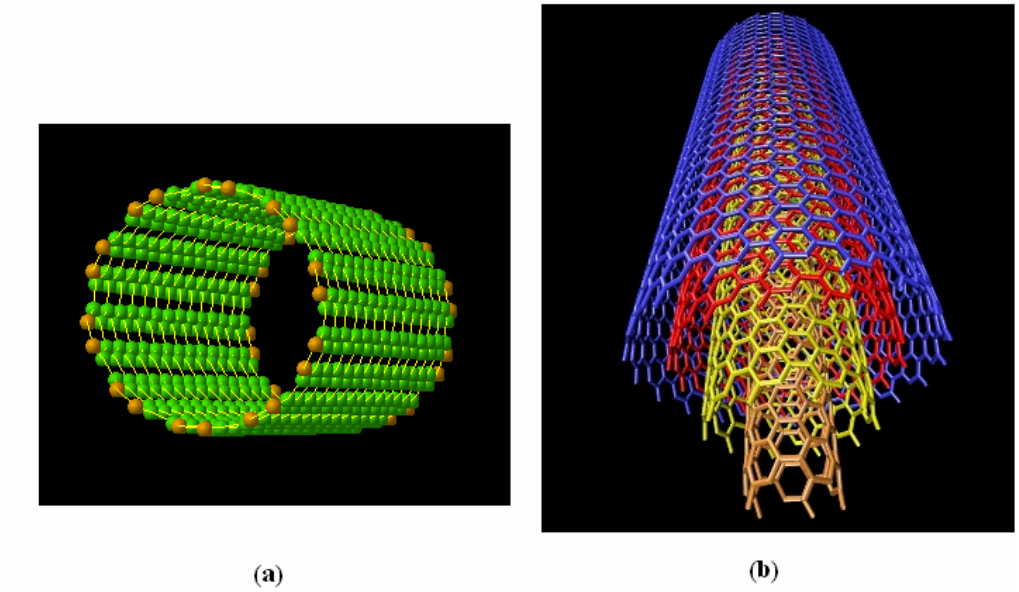

Fig. 1. Single wall carbon nanotube (a) and multiwall carbon nanotube (b)

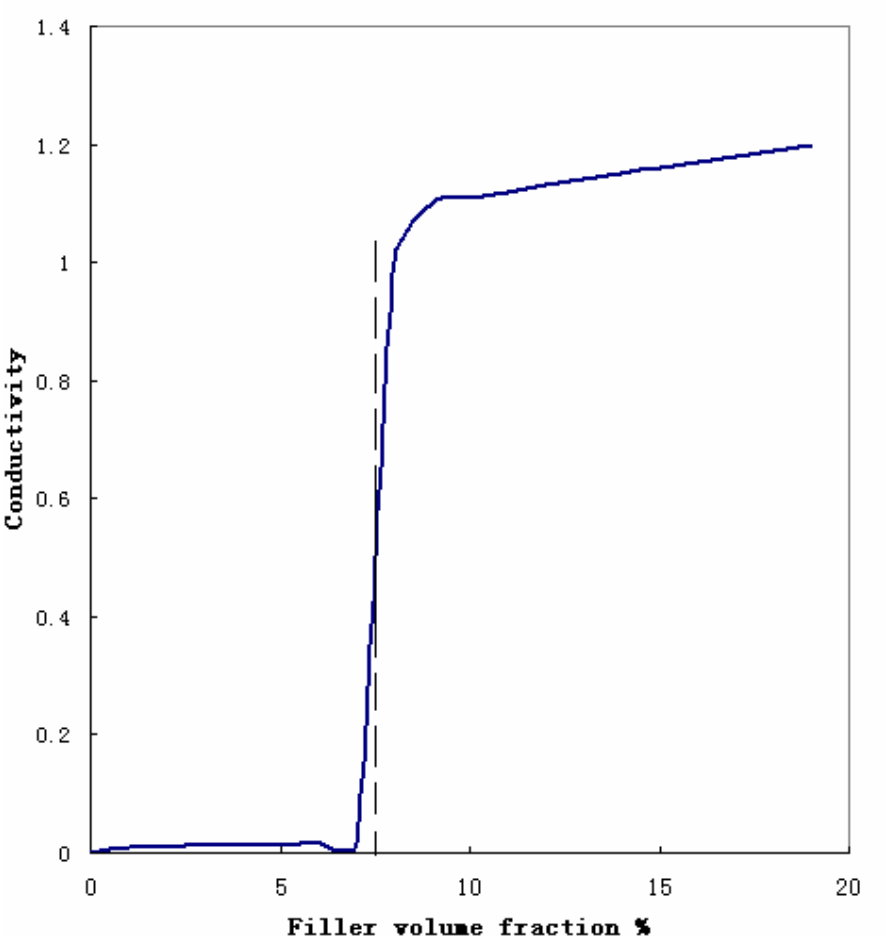

Fig. 2. Insulator-conductor transition characterized by a sharp onset in conductivity

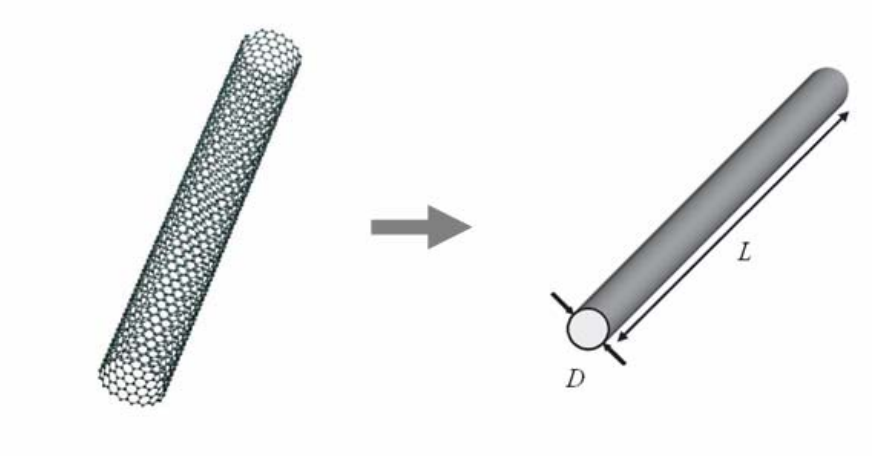

Fig. 3. Equivalent continuum model of carbon nanotubes

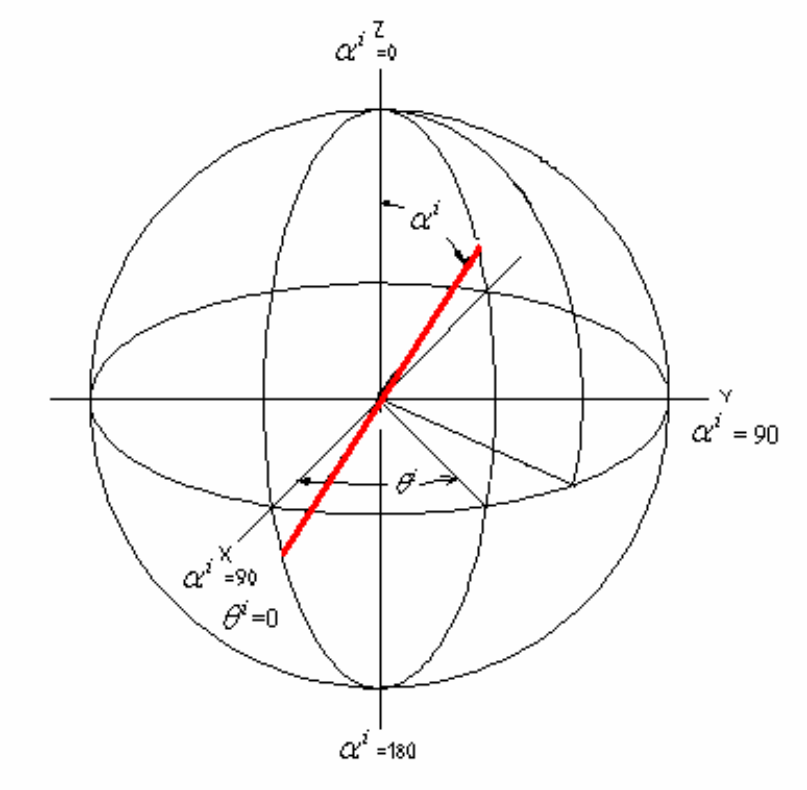

Fig. 4. Local spherical coordinate system for the nano-fiber (red)

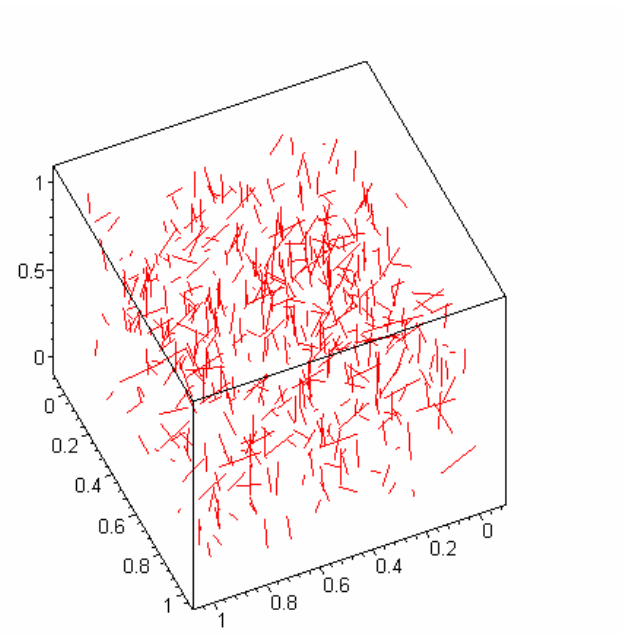

(a)

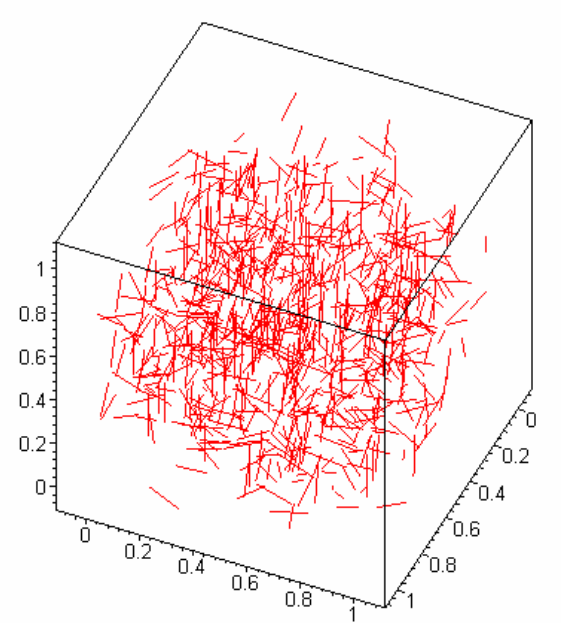

(b)

Fig. 5. Samples with 400(a) and 800(b) fibers distributed randomly; the cube is nondimensional (of unity length) and the normalized fiber length and is 0.1

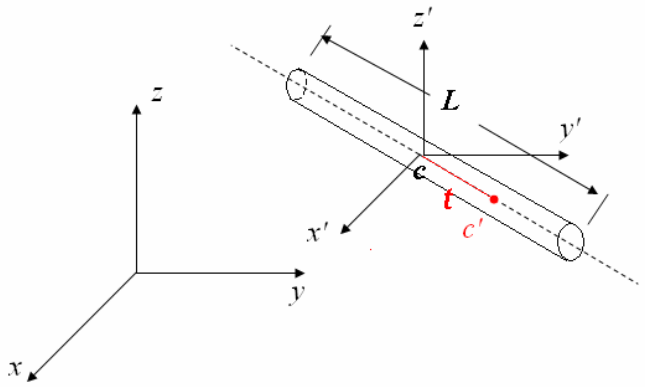

Fig. 6. An arbitrary point on the fiber apart from the fiber center with distance *t*

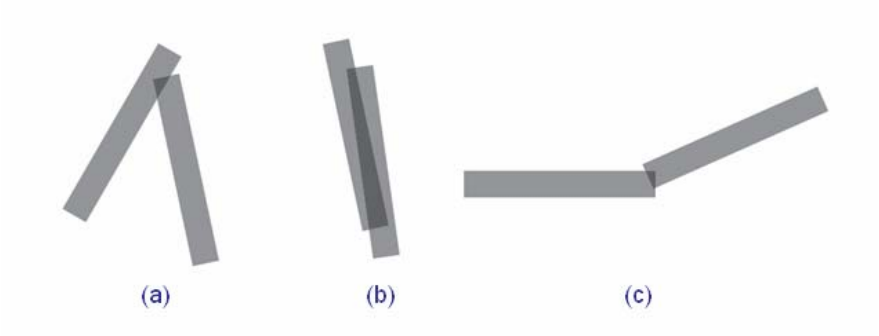

Fig. 7. Different patterns of contact between fiber pairs (a) end-to-side (b) side-to-side (c) end-to-end

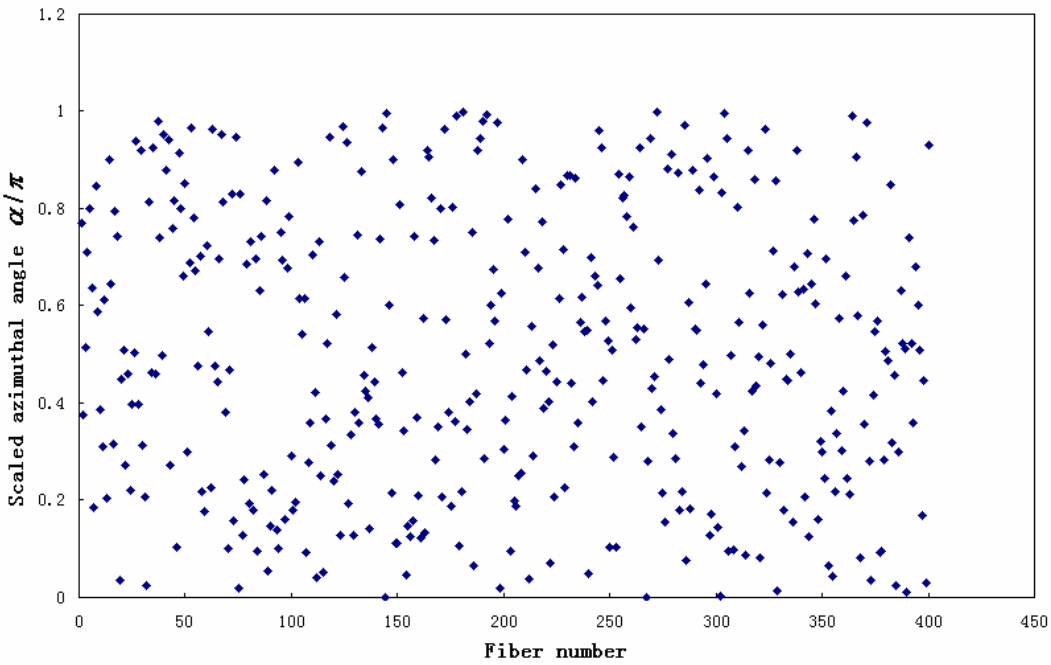

Fig. 8. Random distribution of the fiber azimuthal angles (400 fibers)

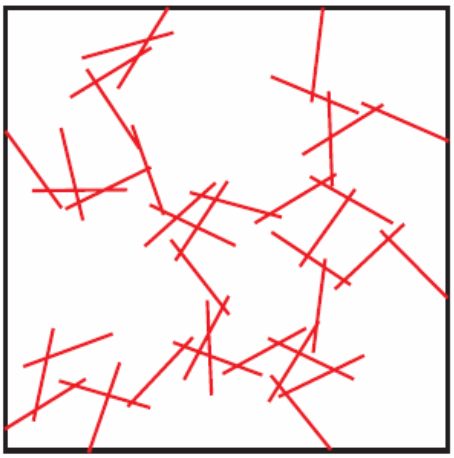

Fig. 9. Network of nanofibers

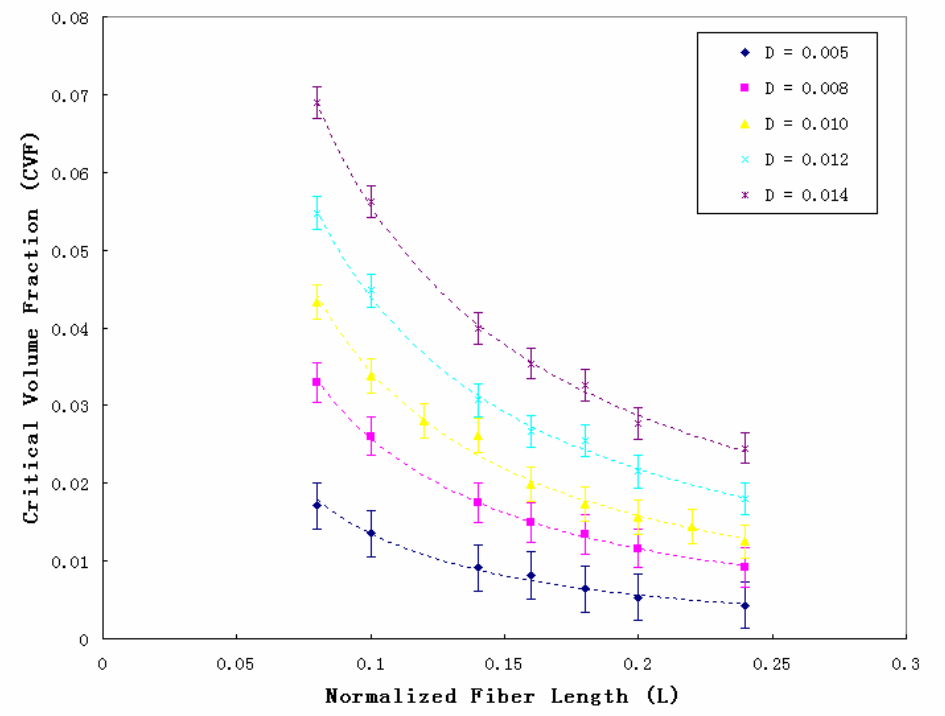

Fig. 10. Effects of fiber diameters and lengths on the critical volume fractions

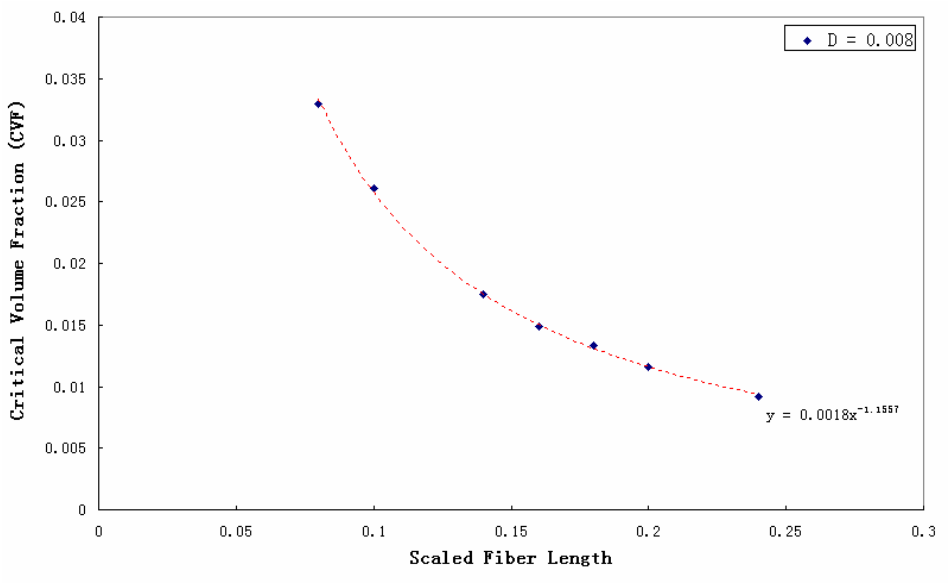

Fig. 11. Critical volume fraction vs. scaled fiber length (fiber diameter =0.008)

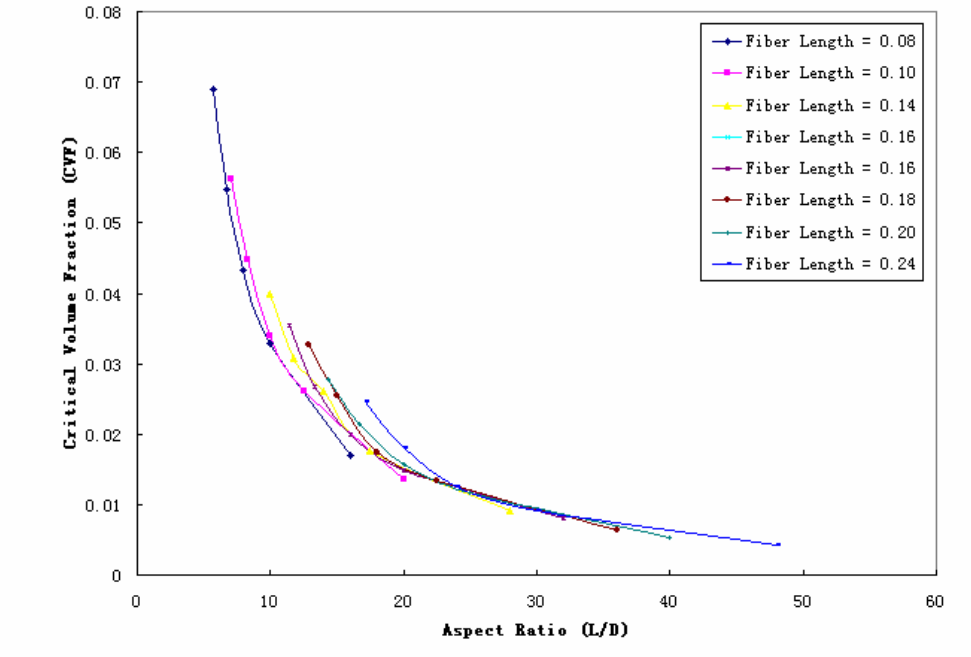

Fig. 12. Critical volume fraction vs. aspect ratio

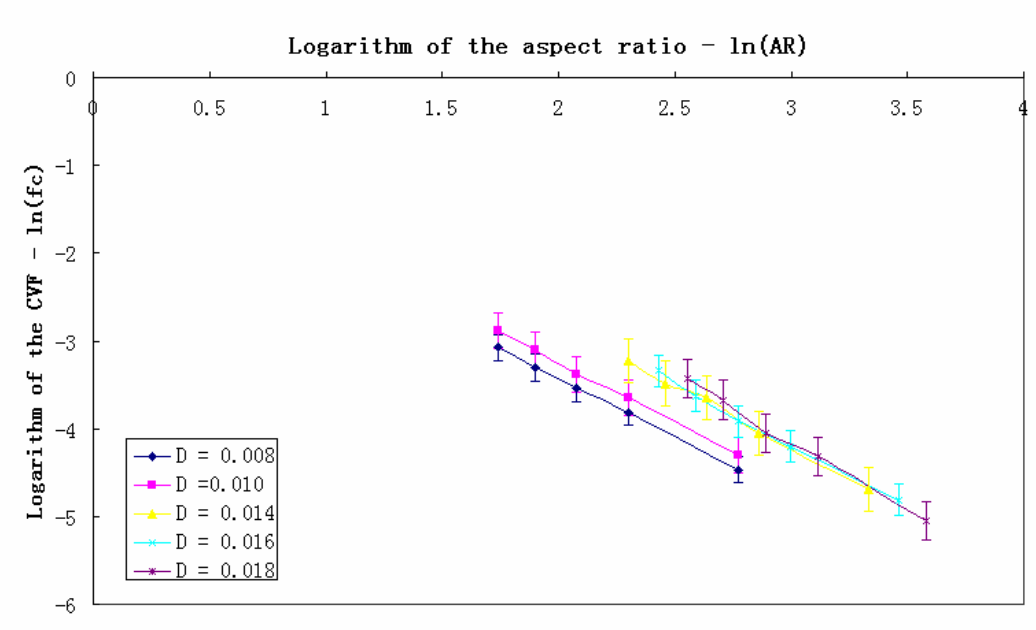

Fig. 13. Plotted logarithms of aspect ratios to critical volume fractions

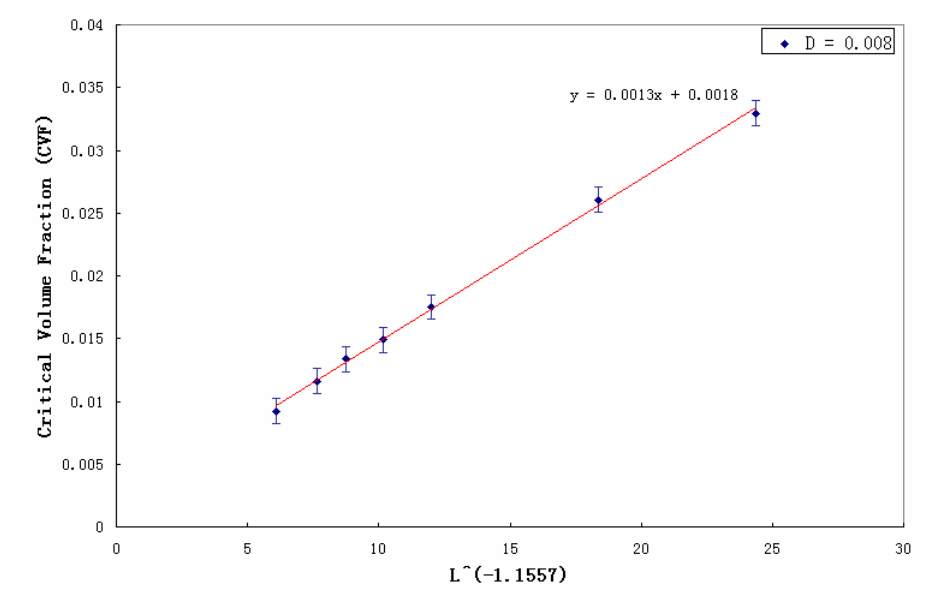

Fig. 14. Linearization of aspect ratios to critical volume fractions

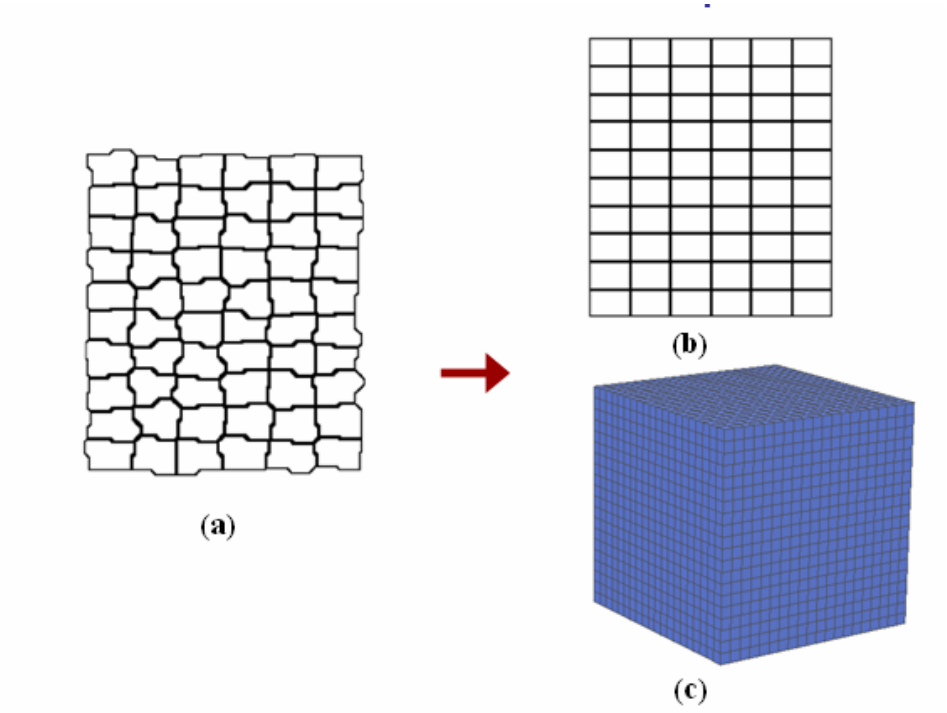

Fig. 15. (a) Real microstructure of irregular emulsion particles; the fibers are only distributed in the interstitial region between fibers; no fibers penetrate the surface of particles; (b,c) A cube matrix representing the emulsion particles; the ratio of interstitial gap width and cube length is 1/10

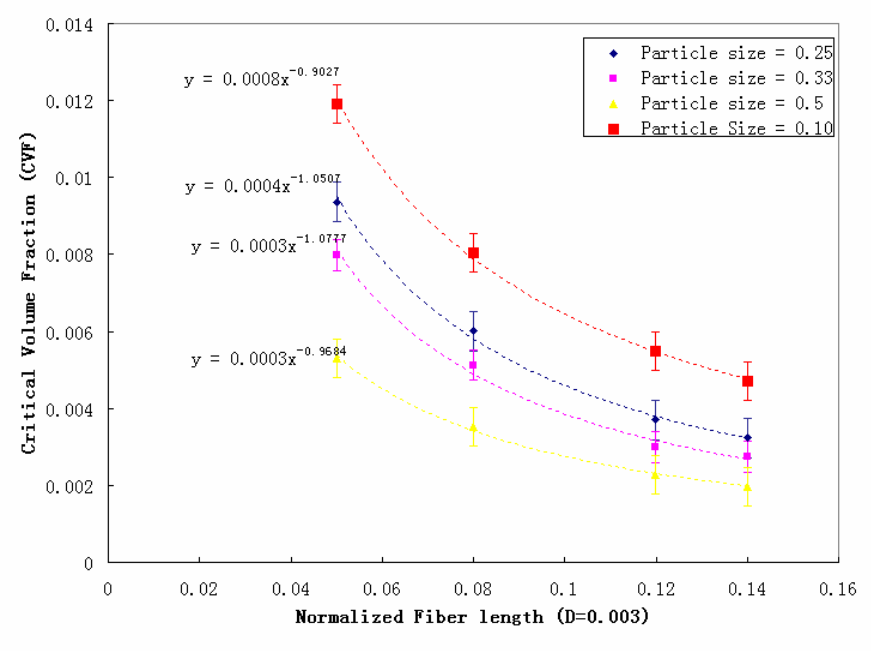

Fig. 16. Normalized fiber length vs. critical volume fraction of samples with emulsion particles (D = 0.003)

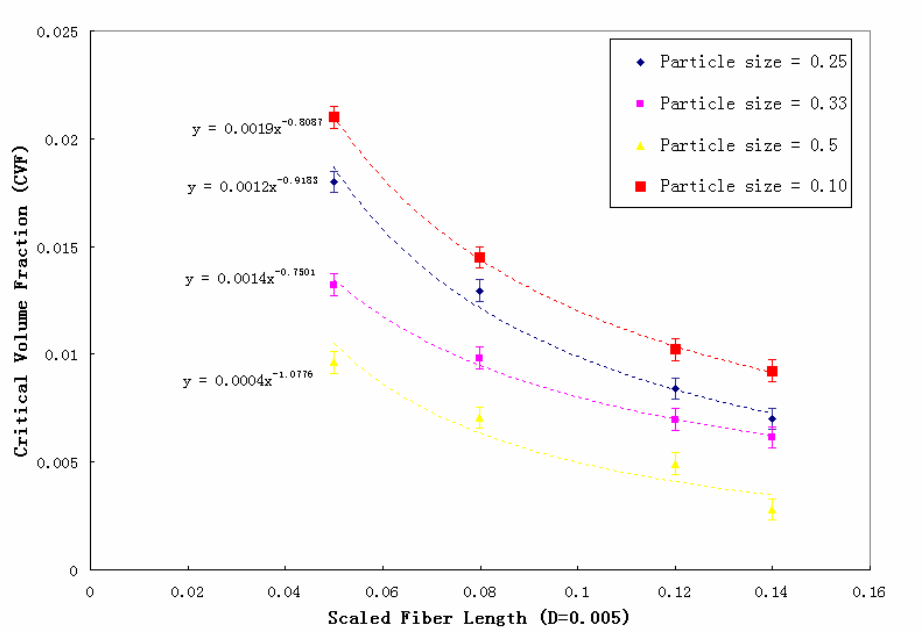

Fig. 17. Normalized fiber length vs. critical volume fraction of samples with emulsion particles (D = 0.005)

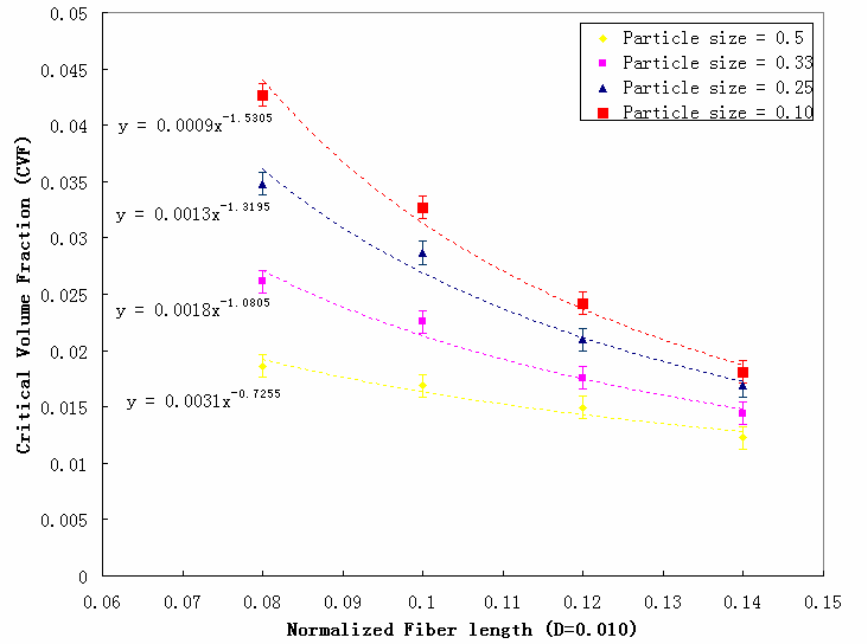

Fig. 18. Normalized fiber length vs. critical volume fraction of samples with emulsion particles (D = 0.010)

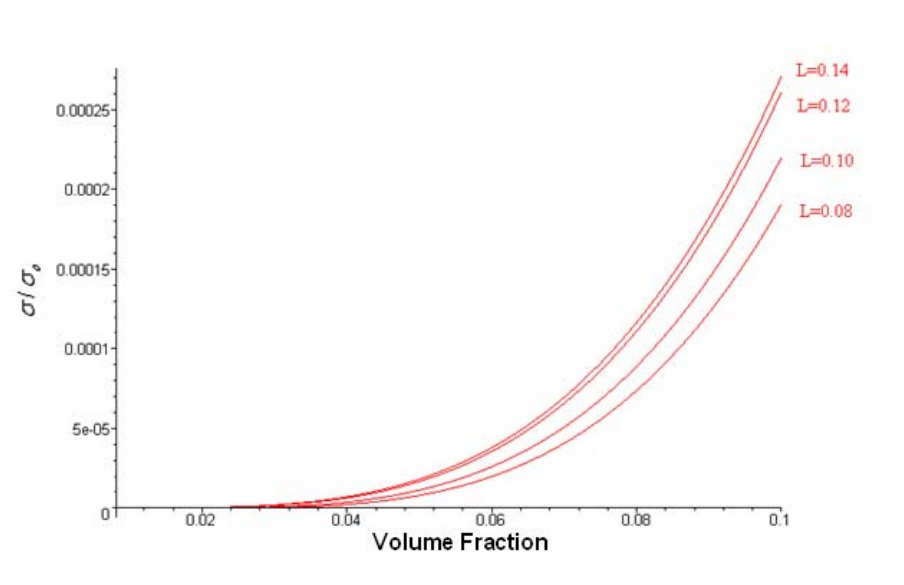

Fig. 19. Samples without emulsion particles (fiber diameter = 0.005)

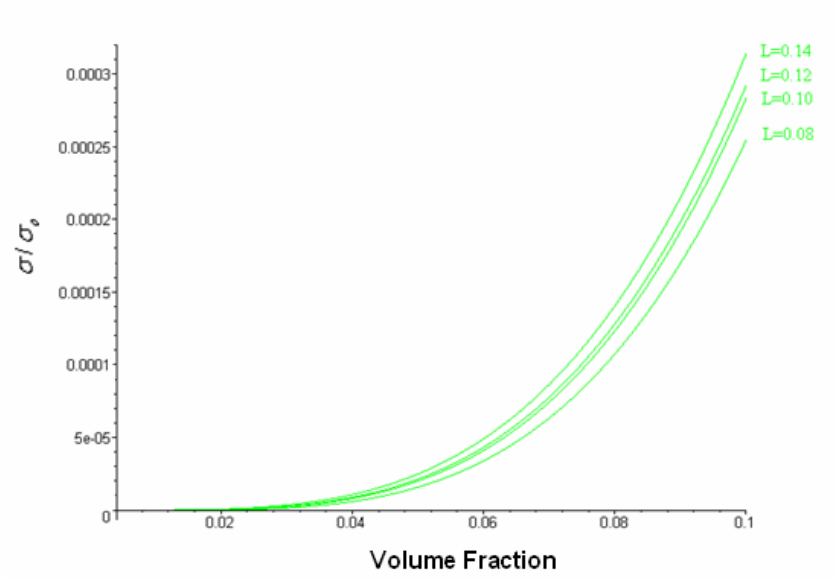

Fig. 20. Samples with emulsion particles (fiber diameter = 0.005)

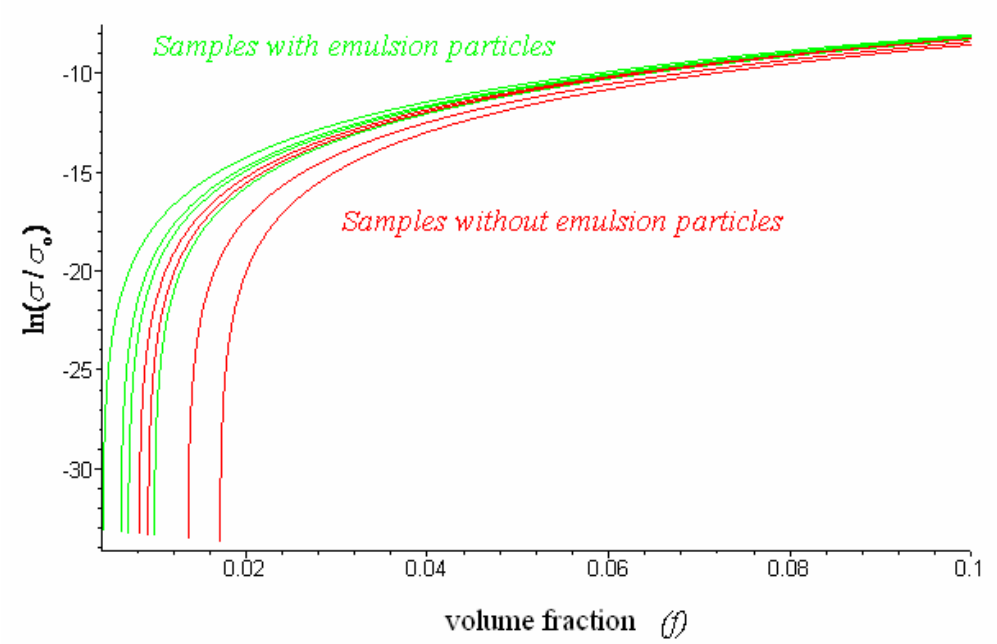

Fig. 21. Logarithm plotting of samples with emulsion particles (fiber diameter = 0.005)

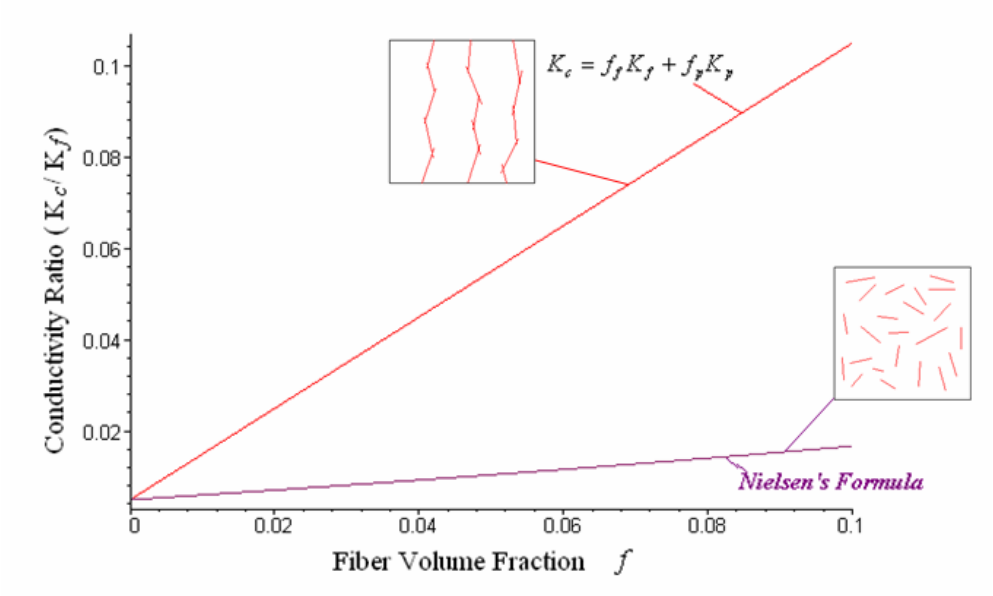

Fig. 22. Plotting of two thermal conductivity equations

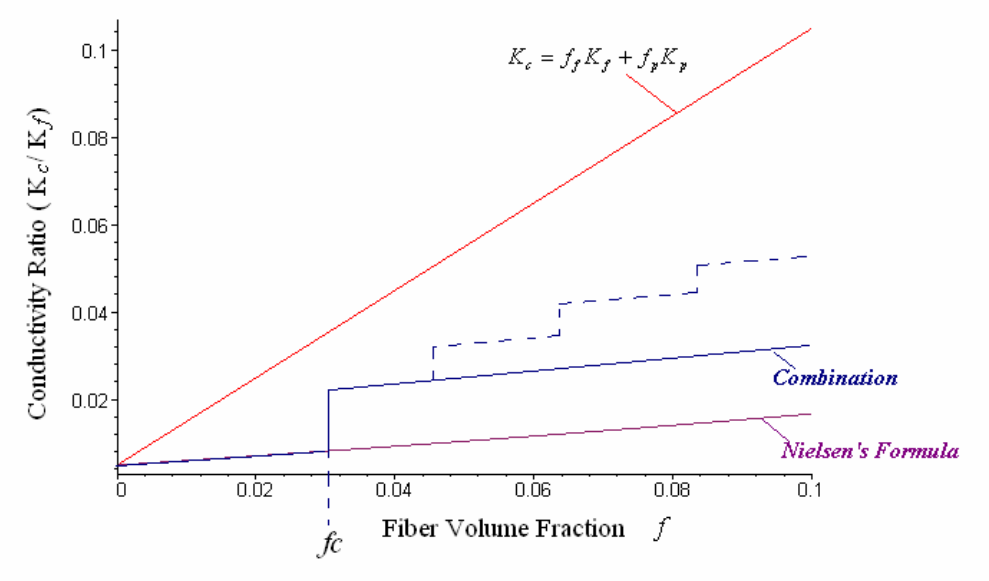

Fig. 23. Combination of two thermal conductivity equations: the blue line represents the real thermal conductivity of the composites with upper bound (red) and lower bound (purple)

APPENDIX B

THE SAMPLE CODES

```
C    SAMPLE CODE #1: A simple random number generator
C
     PROGRAM random
     IMPLICIT none
C
C       declarations
      INTEGER i, number, old, seed, x, y
C
C            set parameters (seed for generator, number of generated numbers)
      seed = 11
      number = 1000
C
C            open output file, seed number generator
      OPEN(6, FILE='rangenf.dat')
      old = seed
C
C            execution
     DO 10 i = 1, number
       x = MOD((57*old+1), 256)
       y = MOD((57*x+1), 256)
       WRITE (6,*) x, y
       old=y
 10   CONTINUE
C
     STOP
     END
```

```
C   SAMPLE CODE #2: A two-dimensional percolation


      SUBROUTINE PERCOLATION (L,N,M,P)
      LOGICAL L(N,M)
      COMMON/CSEED/ ISEED
      DO      200  I = 1, N
        DO    100  J = 1, M
          R = RANF()
          IF(R.LT.P) THEN
            L(I,J) = .TRUE.
          ELSE
            L(I,J) = .FALSE.
          END IF
  100   CONTINUE
  200 CONTINUE
      RETURN
      END
C
      FUNCTION RANF()
      DATA IA/16807/,IC/2147483647/,IQ/127773/,IR/2836/
      COMMON /CSEED/ ISEED
        IH = ISEED/IQ
        IL = MOD(ISEED,IQ)
        IT = IA*IL-IR*IH
        IF(IT.GT.0) THEN
          ISEED = IT
        ELSE
          ISEED = IC+IT
        END IF
        RANF() = ISEED/FLOAT(IC)
      RETURN
      END
```

```
C SAMPLE CODE #3: Integration with the direct sampling Monte Carlo scheme

      PROGRAM MCDS
C
C The integrand is f(x) = x*x.
C
      PARAMETER (M=1000000)
      COMMON /CSEED/ ISEED
      INTEGER*4 time,STIME,T(9)
C
C Initial seed from the system time and forced to be odd
C
      STIME = time(%REF(0))
      CALL gmtime(STIME,T)
      ISEED = T(6)+70*(T(5)+12*(T(4)
     *           +31*(T(3)+23*(T(2)+59*T(1)))))
      IF (MOD(ISEED,2).EQ.0) ISEED = ISEED-1
C
      SUM1 = 0.0
      SUM2 = 0.0
      DO 100 J = 1, M
        X = RANF()
        SUM1 = SUM1+F(X)
        SUM2 = SUM2+F(X)**2
  100 CONTINUE
      S  = SUM1/M
      DS = SQRT(ABS(SUM2/M-(SUM1/M)**2)/M)
      WRITE(6,999) S,DS
      STOP
  999 FORMAT (2F14.8)
      END
C
      FUNCTION F(X)
        F = X*X
      RETURN
      END
C
      FUNCTION RANF()
      DATA IA/16807/,IC/2147483647/,IQ/127773/,IR/2836/
      COMMON /CSEED/ ISEED
        IH = ISEED/IQ
        IL = MOD(ISEED,IQ)
        IT = IA*IL-IR*IH
        IF(IT.GT.0) THEN
          ISEED = IT
        ELSE
```

```
    ISEED = IC+IT
  END IF
  RANF = ISEED/FLOAT(IC)
RETURN
END
```

VITA

Name:	Heng Gu
Address:	Nano-Energy Laboratory Department of Mechanical Engineering, Texas A&M University, College Station, 77843-2123
Email Address:	gh801209@neo.tamu.edu
Education:	B.A., Mechanical & Manufacturing Engineering, Nanjing University of Science & Technology, 2003 M.S., Civil Engineering, Ruhr University Bochum, 2005 M.S., Mechanical Engineering, Texas A&M University, 2008